of liver stiffness. Fibrosis was staged on a 0–4 scale as follows: F0, no fibrosis; F1, portal fibrosis without septa; F2, portal fibrosis and few septa; F3, numerous septa without cirrhosis; F4, cirrhosis. The chronic hepatitis activity was graded as follows: A0, none; A1, mild; A2, moderate; and A3, severe.

Real-time elastography

We used ultrasonography (Hitachi EUB-8500; Hitachi Medical, Chiba, Japan) and an EUP-L52 Linear probe (3–7 MHz; Hitachi Medical) for real-time tissue elastography (RTE). This system is commercially available currently for the diagnosis of mammary neoplasms [17].

Patients were examined in a supine position with the right arm elevated above the head, and were instructed to hold their breath. The examination was performed on the right lobe of the liver through the intercostals, because liver biopsy and Fibroscan were also performed at the same site. The RTE equipment displays two images simultaneously; the RTE image showing the region of interest (ROI) as a colored area and the conventional B-mode image (Fig. 1a). An area was chosen where the tissue was free of large vessels and near the biopsy point. The measurement was fixed to a rectangle with 30 mm length × 20 mm breadth placed 5 mm below the surface of the liver (Fig. 1a). The color in the ROI was graded from blue to red (Fig. 1b). We stored the RTE images as moving digital images for 20–40 s. Then ten static images, captured by the observer at random from the moving images, using AVI2JPG v6.10 converter software (Novo, Tokyo, Japan), were analyzed using the novel software Elasto_ver 1.5.1 (which was developed and donated by Hitachi Medical) on a personal computer. Numerical values of pixels were from 0 to 255 (256 stepwise grading) according to color mapping from blue (0) to red (255), and a histogram of the distribution was generated (Fig. 1c). The scale ranged from red for components with the greatest strain (i.e., softest components) to blue for those with no strain (i.e., hardest components). Green indicated average strain in the ROI, and therefore intact liver tissue displayed a diffuse homogeneous green pattern. An appearance of unevenness in the color pattern was considered to reflect a change in the liver stiffness. For quantification, all pixel data in the colored image were transformed into a histogram and binary image (Fig. 1c, d).

Colored RTE images are usually classified into several patterns in the diagnosis of breast disease [17]. In this study, we evaluated liver fibrosis as three patterns: a diffuse soft pattern, an intermediate pattern, and a patchy hard pattern. The diffuse soft pattern was a relatively homogeneously spread, light-green colored image (Fig. 2a; the corresponding histology is shown in Fig. 2d). The intermediate pattern was typified by a partially mottled, dotted image with blue spots on a light green background (Fig. 2b; the corresponding histology is shown in Fig. 2e). The patchy hard pattern comprised mixed images with a patchwork effect of light green, red, and blue (Fig. 2c; the corresponding histology is shown in Fig. 2f).

Transient elastography

Liver stiffness was also measured by transient elastography (Fibroscan®; Echosens SA, Paris, France). Briefly, patients were placed on the bed in the horizontally supine position. A probe was placed on the skin above the right intercostal space. The velocity of shear waves, which were generated temporarily and passed though the liver, was combined with Young's modulus for the automated calculation of elasticity [9]. Ten successful acquisitions were performed on each patient. The results that obtained ten valid measurements with a success rate of at least 60% and an interquartile range under 30% were considered successful. A median of 10 valid measurements was regarded as the liver stiffness for a given subject, and expressed in kilopascals (kPa).

APRI

The APRI was calculated as follows: aspartate aminotransferase (/upper limit of normal) × 10/platelet count (10^4/mm^3).

Statistical analysis

Box plots were used to study the distribution of the RTE values according to the stage of fibrosis. The trends were evaluated using the Jonckheere–Terpstra test. The Tukey–Kramer test was used to compare the data between the groups. The diagnostic performance of RTE parameters and transient elastography was assessed with receiver operating characteristic (ROC) curves. The ROC curve is a plot of the sensitivity versus 1-specificity for all possible cutoff values. The most commonly used index of accuracy is the area under the receiving operating characteristic curve (AUC), with values close to 1.0 indicating high diagnostic accuracy. Analyses were performed using JMP-8 software (SAS Institute, Cary, USA).

Results

Patients

The characteristics of our 101 patients with chronic HCV infection at the time of RTE and transient elastography are summarized in Table 1. In 91 of them, liver biopsy was performed successfully. Ten patients, who had no clinically

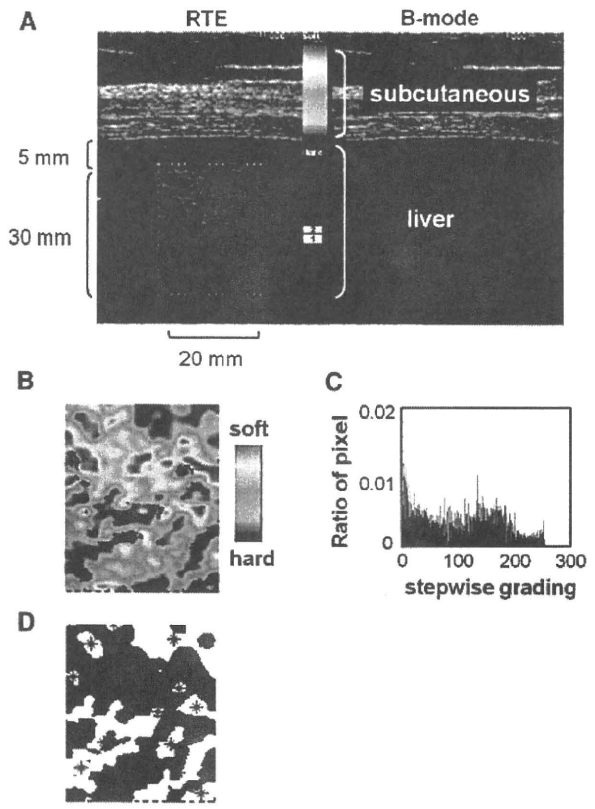

Fig. 1 Procedure of image analyses for real-time tissue elastography (*RTE*). **a** The region of interest (ROI) was fixed to a rectangle with about 30 mm length × about 20 mm breadth with a 400–600 mm^2 area placed 5 mm below the surface of the liver. **b** The color-coded images from the ROI of RTE were analyzed by the software Elasto_ver 1.5.1. The colors ranged from *blue to red*, indicating the relative gradients from hardness to softness. **c** Mean and Standard Deviation were calculated by a histogram, which was generated by 256 stepwise grading derived from the color image obtained in **b**. **d** Area and Complexity were calculated from the binary image. Area was derived from the percentage of *white regions* (*asterisks*, i.e., hard area). Complexity was calculated by the following equation, $periphery^2/Area$. Median value of the data was kept as representative of RTE parameters

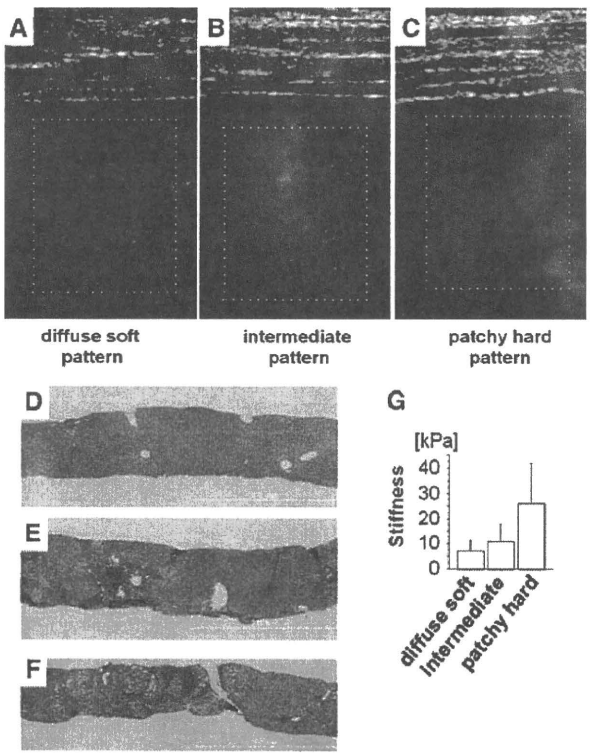

Fig. 2 Representative colored images of real-time tissue elastography. **a** A case of F1 whose histology is shown in **d**. Relatively homogeneous image colored *light green* indicates a diffuse soft pattern in RTE. Liver stiffness measured by transient elastography (Fibroscan) was 4.1 kPa. **b** A case of F3 whose histology is shown in **e**. Partially mottled and dotted image with blue and red spots in the light green background indicates an intermediate pattern in RTE. Liver stiffness measured by Fibroscan was 9.6 kPa. **c** A case of F4 whose histology is shown in **f**. Mixed image with *light green*, *blue*, and *red colors* indicates patchy hard pattern. Liver stiffness measured by Fibroscan was 36.3 kPa. **g** Correlation of the averages of liver stiffness measured by Fibroscan with the three patterns of RTE images. The transition of these three patterns correlated positively with the liver stiffness ($p < 0.01$). **d–f** H&E staining. *Yellow bars* 2 mm

overt sign of decompensated cirrhosis, were diagnosed with cirrhosis (F4) by the appearance of the liver surface at laparoscopy without liver biopsy. RTE was performed successfully in all patients, but five patients (F1, 2; F3, 1; F4, 2) failed to receive transient elastography measurements due to obesity and liver atrophy.

Representative images of real-time tissue elastography

The results were described as the Mean, which indicates the mean of the histogram and ranges from 73.0 to 139.8 (median 111.9), and Standard Deviation (SD), which indicates the standard deviation of the histogram and ranges from 36.5 to 76.6 (median 60.8). In another analysis, the data were transformed into a binary image and the results were described as Area, which indicates the percentage of hard tissue and represents the hard tissue domain divided by the ROI and ranges from 5.0 to 54.7% (median 24.8%), and Complexity, which indicates the complex ratio of the shape of an extracted hard tissue domain in the ROI and is calculated as $periphery^2/area$ of the hard tissue domain and ranges from 15.9 to 40.21 (median 22.9) (Fig. 1d). The four image features were calculated automatically by Elasto_ver 1.5.1 (Hitachi Medical). Mean, SD, and Complexity were described in arbitrary units [a.u.].

The colored RTE images were classified into three patterns according to their visual appearance. The values for liver stiffness measurement by transient elastography (Fibroscan) were 6.9 ± 4.5, 10.9 ± 6.8, and 26.0 ± 15.8 kPa in the diffuse soft pattern group, intermediate pattern group, and patchy

Table 1 Characteristics of the patients at the time of real-time tissue elastography examination

Characteristics	Patients (n = 101)
Sex: male/female	43/58
Age (years)	54 ± 13 (range 24–80)
BMI (kg/m^2)	22.1 ± 3.1 (range 15.1–32.3)
Platelet count (×10^4/mm^3)	16.4 ± 6.6
Total bilirubin (mg/dL)	0.9 ± 0.4
Prothrombin time (INR)	1.02 ± 0.1
ALT (IU/L)	58.2 ± 41.2
Fibrosis stage	
F0	6
F1	48
F2	15
F3	16
F4	16
Histological activity of 91 patients with liver biopsy	
A0	2
A1	24
A2	45
A3	20

Values are means ± SEM

BMI body mass index, *ALT* alanine aminotransferase

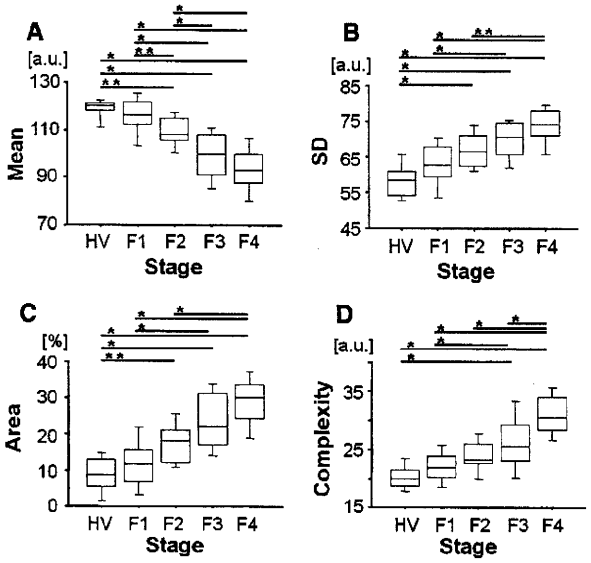

Fig. 3 Parameter analyses measured by real-time tissue elastography (RTE) for each fibrosis stage. Box plots of each RTE value corresponding to fibrosis stages F1–4 and the healthy volunteer group (*HV*). The *tops and bottoms of the boxes* indicate the 1st and 3rd quartiles. The *length of the box* represents the interquartile range within which 50% of values are located. The *lines through the middles of the boxes* represent the medians. **a** Mean, **b** SD, **c** Area, and **d** Complexity. HV, n = 10. F1–4, n = 95. $*p < 0.01$, and $**p < 0.05$

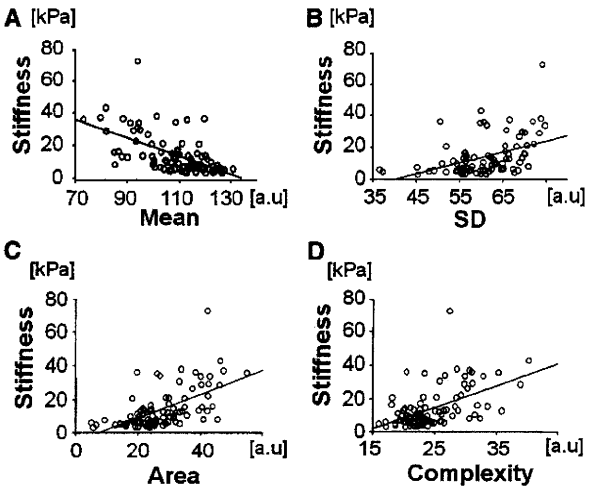

Fig. 4 Correlation between liver stiffness measured by transient elastography (Fibroscan) and the parameters of real-time tissue elastography. **a** Mean was negatively correlated with liver stiffness (kPa) ($p < 0.01$). Correlation coefficient was −0.585. **b** SD was significantly correlated with liver stiffness (kPa) ($p < 0.01$). Correlation coefficient was 0.425. **c** Area was significantly correlated with liver stiffness (kPa) ($p < 0.01$). Correlation coefficient was 0.590. **d** Complexity was significantly correlated with liver stiffness (kPa) ($p < 0.01$). Correlation coefficient was 0.532 (n = 96). *a.u.* arbitrary units

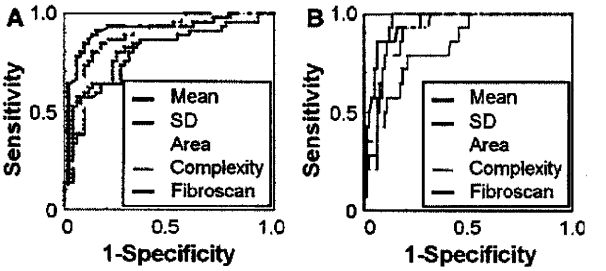

Fig. 5 Receiver operating characteristic curves of each parameter obtained by RTE. **a** No significant fibrosis (F0–1). **b** Cirrhosis (F4). **a** The areas under the receiver operating characteristic curves (AUC) for no significant fibrosis (F0–1) were 0.89, 0.81, 0.87, 0.81, and 0.92 for Mean (*red*), SD (*blue*), Area (*yellow*), Complexity (*pink*), and transient elastography (Fibroscan, *black*), respectively. **b** The AUCs for cirrhosis were 0.91, 0.84, 0.91, 0.93, and 0.95 for Mean, SD, Area, and Complexity, and transient elastography, respectively (n = 96)

hard pattern group, respectively. Thus, these three patterns correlated significantly with the kPa values obtained by transient elastography (Jonckheere–Terpstra test, $p <$ 0.0001) (Fig. 2g).

Relationship between real-time tissue elastography and histological parameters

Figure 3a–d shows box plots of the RTE values corresponding to fibrosis stage and includes the healthy volunteer (HV) group. The Mean decreased with increasing fibrosis

score (Jonckheere–Terpstra test, $p < 0.0001$). SD, Area, and Complexity increased with increasing fibrosis score (Jonckheere–Terpstra test, $p < 0.0001$). The significant differences between each fibrosis stage were as follows: HV versus F3 and F4, F1 versus F3 and F4, and F2 versus F4 at every parameter; HV versus F2 at Mean, SD, and Area; F1 versus F2 at Mean; F2 versus F3 at Mean; F3 versus F4 at Complexity (Tukey–Kramer test, $p < 0.05$) No significant difference was found between the chronic hepatitis activity grades with same fibrosis stage at all parameters (Tukey–Kramer test).

Relationship between real-time tissue elastography and liver stiffness

Figure 4a–d, shows linear regression analysis of the values obtained by RTE compared to the liver stiffness values (kPa) obtained by transient elastography (Fibroscan). Simple regression analyses indicated that Mean, SD, Area, and Complexity were all significantly correlated with liver stiffness measured by Fibroscan (Mean: $r = -0.585$, $p < 0.001$; SD: $r = 0.425$, $p < 0.001$; Area: $r = 0.590$, $p < 0.001$; Complexity: $r = 0.532$, $p < 0.001$).

Relationship between real-time tissue elastography and platelet count, APRI, and other laboratory parameters

Simple regression analyses indicated that all Mean, SD, Area, and Complexity values were significantly correlated with the platelet count (Mean: $r = 0.432$, $p < 0.001$; SD: $r = -0.332$, $p = 0.001$; Area: $r = -0.402$, $p < 0.001$; Complexity: $r = -0.393$, $p < 0.001$). In addition, simple regression analyses indicated that Mean, SD, Area, and Complexity were all significantly correlated with APRI (Mean: $r = -0.442$, $p < 0.001$; SD: $r = 0.373$, $p < 0.001$; Area: $r = 0.425$, $p < 0.001$; Complexity: $r = 0.418$, $p < 0.001$). Furthermore, the correlation coefficient was significant for prothrombin time (Mean: $r = -0.404$, $p < 0.001$; SD: $r = 0.343$, $p < 0.005$; Area: $r = 0.435$, $p < 0.001$; Complexity: $r = 0.440$, $p < 0.001$), while no significant correlation was found for the four image features and total bilirubin, age, BMI, or alanine aminotransferase.

Diagnostic value of real-time tissue elastography and transient elastography

Figure 5 shows the ROC curves of RTE parameters for no significant fibrosis (F0–1) and cirrhosis (F4) in ninety-six patients who were also examined successfully by transient elastography. The AUCs for the stage of no significant fibrosis (F0–1) were 0.89, 0.81, 0.87, and 0.81 for Mean, SD, Area, and Complexity, respectively. The AUCs for severe fibrosis (≥F3) were 0.93, 0.84, 0.91, and 0.86 for Mean, SD, Area, and Complexity, respectively. The AUCs for cirrhosis (F4) were 0.91, 0.84, 0.91, and 0.93 for Mean, SD, Area, and Complexity, respectively. In transient elastography (Fibroscan), the AUCs were 0.92, 0.95, and 0.95 for stages F0–1, ≥F3s and F4, respectively. The corresponding sensitivities, specificities, and positive and negative predictive values are detailed in Table 2.

Discussion

Recently, various techniques based on ultrasound or magnetic resonance imaging have been developed to quantify

Table 2 Cutoff values of real-time tissue elastography (image features) and transient elastography for the diagnosis of fibrosis stages (*F*)

	$F = 0$–1	$F \geq 3$	$F = 4$
Mean (AUC)	0.89	0.93	0.91
Cutoff (a.u.)	110.1	106.9	101.5
Sensitivity (%)	84.1	82.8	85.7
Specificity (%)	82.7	85.1	82.9
Positive predictive value (%)	80.4	70.6	46.2
Negative predictive value (%)	86.0	91.9	97.1
SD (AUC)	0.81	0.84	0.84
Cutoff (a.u.)	61.2	63.0	65.7
Sensitivity (%)	70.5	75.9	78.6
Specificity (%)	73.1	77.6	79.3
Positive predictive value (%)	68.9	59.5	39.3
Negative predictive value (%)	74.5	88.1	95.6
Area (AUC)	0.87	0.91	0.91
Cutoff (%)	25.8	29.5	33.7
Sensitivity (%)	81.8	79.3	85.7
Specificity (%)	80.8	80.6	86.6
Positive predictive value (%)	78.3	63.9	52.2
Negative predictive value (%)	79.6	90.0	97.3
Complexity (AUC)	0.81	0.86	0.93
Cutoff (a.u.)	23.2	24.9	27.8
Sensitivity (%)	77.3	79.3	85.7
Specificity (%)	75.0	80.6	87.8
Positive predictive value (%)	72.3	63.9	54.5
Negative predictive value (%)	79.6	90.0	97.3
Transient elastography (AUC)	0.92	0.95	0.95
Cutoff (kPa)	10.1	13.3	16.3
Sensitivity (%)	88.6	89.7	85.7
Specificity (%)	86.5	86.6	85.4
Positive predictive value (%)	84.8	74.3	50.0
Negative predictive value (%)	90.0	95.1	97.2

AUC the area under the receiver operating characteristic curves, *a.u.* arbitrary units

liver stiffness, and thereby liver fibrosis, noninvasively. Among them, transient elastography (Fibroscan) has been used most frequently worldwide and has become established in clinical practice to detect advanced fibrosis without liver biopsy, although several limitations and disadvantages of the modality have been discussed [8, 24]. Another novel imaging modality is magnetic resonance elastography (MRE). The technique typically is added to a conventional MR examination of the upper abdomen [25]. A pneumatic or electromechanical driver is placed in contact with the abdominal wall and is used to generate propagating mechanical waves in the liver at frequencies between 40 and 120 Hz. Although MRE was shown to be superior to APRI and transient elastography for determining the stage of fibrosis in patients with various underlying liver diseases [26], MRE cannot be performed on an iron-overloaded liver because of noise. In addition, MRE takes a longer time and costs more than the ultrasound-based elastographies [2].

We paid attention in our analysis to the pattern change of RTE color images according to the progression of fibrosis. Normal or minimally fibrotic liver exhibited a homogeneous RTE image that was colored light green (Fig. 2a). According to the progression of liver fibrosis, the homogeneous pattern transited to a patchy pattern consisting of a blue-colored area (Fig. 2c), which may suggest a collapse of homogeneity. In the present study, for semi-quantification of the RTE image, we used a histogram and binary image produced using an exclusive software program that was developed by Hitachi Medical. This is the first report demonstrating the utility of Mean, SD, Area, and Complexity as RTE parameters. We speculate that Mean and Area may directly represent liver elasticity, while SD and Complexity may imply the collapse of the uniform architecture of the liver parenchyma concomitant with progressing hepatic fibrosis (Figs. 3, 5).

After the report by Friedrich-Rust et al. [21] other investigators criticized the intraobserver variability and the lack of interobserver agreement in hepatic RTE [27–29]. In general practice, an operator presses lightly on the surface of the liver through the skin with a transducer when the elastogram is generated. Thus, the pressure generated by the operator's compression is assumed to influence both the image of elasticity and the resulting elasticity score. To avoid this source of error, we used here the latest and most sensitive probe that was produced by Hitachi Medical and did not require extra external stress. Accordingly, we were able to improve the acquisition of the color image representing the distortion of liver tissue under the heartbeat or abdominal aorta. We also adopted ten individual frames for semi-quantitative analysis. On the other hand, Saftoiu et al. and Gulizia et al. have proposed that the ROI should include the surrounding tissues, such as adipose tissue, diaphragm, and intercostal muscles, in order to clearly compare and distinguish the strain between the liver and these organs [27, 30]. However, we placed the ROI inside the liver at 5 mm below the surface of the liver, because the new probe used in this study is sensitive and the deep attenuation of the ultrasound image could be disregarded. We avoided including the liver surface inside the ROI because the liver surface is hard and therefore is assessed as a harder area, influencing the histogram analysis. Recently, Tatsumi et al. [31] also reported the results of RTE using the ROI inside the liver in a similar fashion to our study.

We note that all four image features of RTE, comprising Mean, SD, Area, and Complexity, were significantly correlated with the kPa value obtained by Fibroscan [8, 11–13]. In particular, Mean and Area had a high correlation. In addition, the AUC values were similar between RTE and Fibroscan. Mean and Area were highly accurate for the diagnosis of significant fibrosis (i.e., >F0–1) and for the diagnosis of cirrhosis (F4). Although the performance of Fibroscan has been demonstrated in many studies to have high accuracy [4, 8], the machine is used solely for elasticity measurements. In contrast, with the new equipment used in the present study, RTE can be used simultaneously with conventional B-mode ultrasonography. Moreover, as reported by Obara et al. [32], liver stiffness measurement by Fibroscan was unsuccessful in 5.3% of Japanese cases of chronic liver disease, similar to our experience in the present study (5.0%). Thus, RTE is considered to be superior to Fibroscan at points where measurements by Fibroscan are difficult to perform in obese patients and are impossible to perform in patients with ascites [32, 33], and where RTE images are unaffected by steatosis, as suggested previously by Friedrich-Rust et al. [29]. Furthermore, because Fibroscan measures liver stiffness between 25 and 65 mm below the surface of the skin [10], knowledge of the relative thickness of the liver is necessary for the measurements.

The diagnostic performance of RTE is similar to that of other noninvasive laboratory tests, such as the FibroTest (BioPredictive, Paris, France), APRI, and the Forns score reported in the literature [4, 8]. The FibroTest is based on five serological parameters; bilirubin, gamma-glutamyl transpeptidase (GGT), apolipoprotein A1, α2-macroglobulin, and haptoglobin. While the diagnostic accuracy was high (AUC 0.87) for significant fibrosis (METAVIR, ≥F2), the FibroTest costs more than APRI and the Forns score, and needs two uncommon parameters [34]. In APRI, using the cutoffs proposed by Wai et al. [5], approximately 50% of patients could be correctly classified as having cirrhosis without a liver biopsy5. With the Forns' index, the AUC for the prediction of significant fibrosis (Scheuer classification, ≥F2) was 0.86 in the test set and 0.81 in the validation set [35]. It is, however, known that the determination of the

severity of liver fibrosis by serum markers is confounded by acute inflammation, hemolysis, cholestasis, and renal failure [4, 5, 34, 35]. Castera et al. [11] compared the performance of transient elastography with that of the FibroTest, APRI, and liver biopsy for the assessment of liver fibrosis in a large number of patients with hepatitis C. Interestingly, they reported that the best performance was achieved by a combination of transient elastography with the FibroTest [11]. Friedrich-Rust et al. reported that the best diagnostic accuracy was obtained by combining the variables used for the calculation of the RTE elasticity score with the platelet count and GGT [18]. Thus, RTE, in combination with serological parameters, can further improve the accuracy of differentiating fibrosis stages.

One of the major limitations of the present study was that the number of patients with F1 was higher than the number of those with the other stages, because most of our patients received liver biopsy prior to interferon treatment. However, our study compared the performance of RTE with that of transient elastography in the same patients. Although the AUC for RTE in this study was higher than that in the studies by Friedrich-Rust et al. [21, 29], the AUC for transient elastography was approximately equivalent to that in one of these studies [29].

In the METAVIR and Desmet's histological scoring systems, cirrhosis is classified as a single category (i.e., F4) [22, 23]. However, the degree of fibrosis; for example, the content of collagen and extracellular matrix materials that may be closely associated with the function of hepatocytes and portal hypertension, may vary among patients with cirrhosis. Foucher et al. [36] reported that the kPa measured by transient elastography in cirrhotic patients correlated well with clinical parameters indicating the severity of cirrhosis; 27.5 kPa was the cutoff value for the presence of esophageal varices stage 2 or 3, 37.5 kPa for liver function Child B or C, 49.1 kPa for a past history of ascites, and 62.7 kPa for esophageal variceal bleeding. Thus, because cirrhosis can be staged in greater detail with clinical relevance based on liver stiffness with RTE, RTE may be useful for this staging of cirrhosis and for detecting and assessing the risk of cirrhotic complications [36].

In summary, we have shown a convenient and noninvasive procedure, RTE, for the visual assessment of liver stiffness. The performance of RTE compares favorably with that of transient elastography (Fibroscan) for detecting the presence of significant liver fibrosis in patients with chronic hepatitis C. We suggest that RTE could be used as a routine imaging method to evaluate the degree of liver fibrosis in patients with liver disease. Future studies of larger patient cohorts will be necessary for the validation of the four RTE parameters, and the combination of these parameters will enable improvement of accuracy in assessing hepatic fibrosis.

Acknowledgments We thank Ms. Akiko Tonomura and Mr. Junji Warabino, Hitachi Medical Co., for the technical support for RTE. Hiroyasu Morikawa was supported by a research grant from Osaka City University (2009). Norifumi Kawada was supported by Research on Hepatitis, Health and Labour Science Research Grants from the Ministry of Health, Labour and Welfare of Japan (2008–2009) and by a Thrust Area Research Grant from Osaka City University (2008–2009).

References

1. Global surveillance and control of hepatitis C. Report of a WHO Consultation organized in collaboration with the Viral Hepatitis Prevention Board, Antwerp, Belgium. J Viral Hepat. 1999;6:35–47.
2. Manns MP, McHutchison JG, Gordon SC, Rustgi VK, Shiffman M, Reindollar R, et al. Peginterferon alfa-2b plus ribavirin compared with interferon alfa-2b plus ribavirin for initial treatment of chronic hepatitis C: a randomised trial. Lancet. 2001;358:958–65.
3. Sporea I, Popescu A, Sirli R. Why, who and how should perform liver biopsy in chronic liver diseases. World J Gastroenterol. 2008;14:3396–402.
4. Manning DS, Afdhal NH. Diagnosis and quantitation of fibrosis. Gastroenterology. 2008;134:1670–81.
5. Wai CT, Greenson JK, Fontana RJ, Kalbfleisch JD, Marrero JA, Conjeevaram HS, et al. A simple noninvasive index can predict both significant fibrosis and cirrhosis in patients with chronic hepatitis C. Hepatology. 2003;38:518–26.
6. Sandrin L, Tanter M, Gennisson JL, Catheline S, Fink M. Shear elasticity probe for soft tissues with 1D transient elastography. IEEE Trans Ultrason Ferroelectr Freq Control. 2002;49:436–46.
7. Ganne-Carrié N, Ziol M, de Ledinghen V, Douvin C, Marcellin P, Castera L, et al. Accuracy of liver stiffness measurement for the diagnosis of cirrhosis in patients with chronic liver diseases. Hepatology. 2006;44:1511–7.
8. Pinzani M, Vizzutti F, Arena U, Marra F. Technology Insight: noninvasive assessment of liver fibrosis by biochemical scores and elastography. Nat Clin Pract Gastroenterol Hepatol. 2008;5:95–106.
9. Yeh WC, Li PC, Jeng YM, Hsu HC, Kuo PL, Li ML, et al. Elastic modulus measurements of human liver and correlation with pathology. Ultrasound Med Biol. 2002;28:467–74.
10. Sandrin L, Fourquet B, Hasquenoph JM, Yon S, Fournier C, Mal F, et al. Transient elastography: a new noninvasive method for assessment of hepatic fibrosis. Ultrasound Med Biol. 2003;29:1705–13.
11. Castéra L, Vergniol J, Foucher J, Le Bail B, Chanteloup E, Haaser M, et al. Prospective comparison of transient elastography, Fibrotest, APRI, and liver biopsy for the assessment of fibrosis in chronic hepatitis C. Gastroenterology. 2005;128:343–50.
12. Ziol M, Handra-Luca A, Kettaneh A, Christidis C, Mal F, Kazemi F, et al. Noninvasive assessment of liver fibrosis by measurement of stiffness in patients with chronic hepatitis C. Hepatology. 2005;41:48–54.
13. Friedrich-Rust M, Ong MF, Martens S, Sarrazin C, Bojunga J, Zeuzem S, et al. Performance of transient elastography for the staging of liver fibrosis: a meta-analysis. Gastroenterology. 2008;134:960–74.
14. Arena U, Vizzutti F, Corti G, Ambu S, Stasi C, Bresci S, et al. Acute viral hepatitis increases liver stiffness values measured by transient elastography. Hepatology. 2008;47:380–4.
15. Nitta N, Yamakawa M, Shiina T. Tissue elasticity imaging based on combined autocorrelation method and 3D tissue model. In: Proceedings of the IEEE Ultrasonics Symposium. Savoy, Ill:

Institute of Electrical and Electronics Engineers Ultrasonics, Ferroelectrics, and Frequency Control Digital Archive 1998, vol. 2, p. 1447–50.
16. Yamakawa M, Shiina T. Strain estimation using the extended combined autocorrelation method. Jpn J Appl Phys. 2001;40:3872–6.
17. Itoh A, Ueno E, Tohno E, Kamma H, Takahashi H, Shiina T, et al. Breast disease: clinical application of US elastography for diagnosis. Radiology. 2006;239:341–50.
18. Tohno E, Ueno E. Current improvements in breast ultrasound, with a special focus on elastography. Breast Cancer. 2008;15:200–4.
19. Tsutsumi M, Miyagawa T, Matsumura T, Kawazoe N, Ishikawa S, Shimokama T, et al. The impact of real-time tissue elasticity imaging (elastography) on the detection of prostate cancer: clinicopathological analysis. Int J Clin Oncol. 2007;12:250–5.
20. Uchida H, Hirooka Y, Itoh A, Kawashima H, Hara K, Nonogaki K, et al. Feasibility of tissue elastography using transcutaneous ultrasonography for the diagnosis of pancreatic diseases. Pancreas. 2009;38:17–22.
21. Friedrich-Rust M, Ong MF, Herrmann E, Dries V, Samaras P, Zeuzem S, et al. Real-time elastography for noninvasive assessment of liver fibrosis in chronic viral hepatitis. AJR Am J Roentgenol. 2007;188:758–64.
22. Desmet VJ, Gerber M, Hoofnagle JH, Manns M, Scheuer PJ. Classification of chronic hepatitis: diagnosis, grading and staging. Hepatology. 1994;19:1513–20.
23. The French Metavir Cooperative Study Group. Intraobserver and interobserver variations in liver biopsy interpretation in patients with chronic hepatitis C. Hepatology. 1994;20:15–20.
24. Bonekamp S, Kamel I, Solga S, Clark J. Can imaging modalities diagnose and stage hepatic fibrosis and cirrhosis accurately? J Hepatol. 2009;50:17–35.
25. Muthupillai R, Lomas DJ, Rossman PJ, Greenleaf JF, Manduca A, Ehman RL. Magnetic resonance elastography by direct visualization of propagating acoustic strain waves. Science. 1995;269:1854–7.
26. Huwart L, Sempoux C, Vicaut E, Salameh N, Annet L, Danse E, et al. Magnetic resonance elastography for the noninvasive staging of liver fibrosis. Gastroenterology. 2008;135:32–40.
27. Săftoiu A, Gheonea DI, Ciurea T. Hue histogram analysis of real-time elastography images for noninvasive assessment of liver fibrosis (letter). AJR Am J Roentgenol. 2007;189:W232–3.
28. Ferraioli G, Gulizia R, Filice C. Real-time elastography in the assessment of liver fibrosis (letter). AJR Am J Roentgenol. 2007;189:W170.
29. Friedrich-Rust M, Schwarz A, Ong M, Dries V, Schirmacher P, Herrmann E, et al. Real-time tissue elastography versus FibroScan for noninvasive assessment of liver fibrosis in chronic liver disease. Ultraschall Med. 2009;30:478–84.
30. Gulizia R, Ferraioli G, Filice C. Open questions in the assessment of liver fibrosis using real-time elastography. AJR Am J Roentgenol. 2008;190:W370–1.
31. Tatsumi C, Kudo M, Ueshima K, Kitai S, Ishikawa E, Yada N, et al. Non-invasive evaluation of hepatic fibrosis for type C chronic hepatitis. Intervirology. 2010;53:76–81.
32. Obara N, Ueno Y, Fukushima K, Nakagome Y, Kakazu E, Kimura O, et al. Transient elastography for measurement of liver stiffness measurement can detect early significant hepatic fibrosis in Japanese patients with viral and nonviral liver diseases. J Gastroenterol. 2008;43:720–8.
33. Ogawa E, Furusyo N, Toyoda K, Takeoka H, Otaguro S, Hamada M, et al. Transient elastography for patients with chronic hepatitis B and C virus infection: non-invasive, quantitative assessment of liver fibrosis. Hepatol Res. 2007;37:1002–10.
34. Imbert-Bismut F, Ratziu V, Pieroni L, Charlotte F, Benhamou Y, Poynard T, et al. Biochemical markers of liver fibrosis in patients with hepatitis C virus infection: a prospective study. Lancet. 2001;357:1069–75.
35. Forns X, Ampurdanès S, Llovet JM, Aponte J, Quintó L, Martínez-Bauer E, et al. Identification of chronic hepatitis C patients without hepatic fibrosis by a simple predictive model. Hepatology. 2002;36:986–92.
36. Foucher J, Chanteloup E, Vergniol J, Castéra L, Le Bail B, Adhoute X, et al. Diagnosis of cirrhosis by transient elastography (FibroScan): a prospective study. Gut. 2006;55:403–8.

See related Commentary on page 10

The American Journal of Pathology, Vol. 177, No. 1, July 2010
Copyright © American Society for Investigative Pathology
DOI: 10.2353/ajpath.2010.090895

Gastrointestinal, Hepatobiliary and Pancreatic Pathology

A Human-Type Nonalcoholic Steatohepatitis Model with Advanced Fibrosis in Rabbits

Tomohiro Ogawa,* Hideki Fujii,*
Katsutoshi Yoshizato,*† and Norifumi Kawada*

From the Department of Hepatology, Graduate School of Medicine, Osaka City University, Osaka; and PhoenixBio Co. Ltd.,† Hiroshima, Japan*

Nonalcoholic steatohepatitis (NASH) progresses to liver fibrosis and cirrhosis, which can lead to life-threatening liver failure and the development of hepatocellular carcinoma. The aim of the present study was to create a rabbit model of NASH with advanced fibrosis (almost cirrhosis) by feeding the animals a diet supplemented with 0.75% cholesterol and 12% corn oil. After 9 months of feeding with this diet, the rabbits showed high total cholesterol levels in serum and liver tissues in the absence of insulin resistance. The livers became whitish and nodular. In addition, the number of rabbit macrophage antigen-positive cells and the expression of mRNAs for inflammatory cytokines showed a significant increase. Moreover, fibrotic septa composed of collagens and α-smooth muscle actin-positive cells were found between the central and portal veins, indicating alteration of the parenchymal architecture. There was also a marked increase of mRNAs for transforming growth factor-β1 and collagen 1A1. Comprehensive analysis of protein and gene expression revealed an imbalance of the antioxidant system and methionine metabolism. We also found that ezetimibe attenuated steatohepatitis in this model. In conclusion, the present rabbit model of NASH features advanced fibrosis that is close to cirrhosis and may be useful for analyzing the molecular mechanisms of human NASH. Ezetimibe blunted the development of NASH in this model, suggesting its potential clinical usefulness for human steatohepatitis. ***(Am J Pathol 2010, 177:153–165; DOI: 10.2353/ajpath.2010.090895)***

A high-fat diet is one of the risk factors for metabolic syndrome, which is characterized by obesity, hyperlipidemia, hyperglycemia, and hypertension, and is frequently accompanied by life-threatening arteriosclerosis.[1] A high-calorie, high-fat diet is also considered to cause nonalcoholic fatty liver disease (NAFLD), which covers a spectrum of disorders from simple steatosis to nonalcoholic steatohepatitis (NASH) and cirrhosis.[2–5] Recent clinical studies have shown that NAFLD is one of the common liver diseases that leads to cirrhosis and hepatocellular carcinoma[2] in a manner similar to the clinical course of chronic viral hepatitis and alcohol abuse.[6] However, the molecular mechanisms underlying the progression of NAFLD to an advanced stage with active inflammation and fibrosis are not fully understood. We recently reported a rabbit model of steatohepatitis that was generated by feeding the rabbit a high-fat and -cholesterol diet (HFD) supplemented with 20% corn oil and 1.25% (w/w) cholesterol for 8 weeks.[7] The rabbit showed insulin resistance, accumulation of lipids in hepatocytes, activation of Kupffer cells (liver macrophages), mild fibrosis, and enhanced oxidative stress. Thus, we concluded that this model was useful for analyzing the molecular mechanisms involved in the pathogenesis of human NASH. However, rabbits fed a HFD have a short lifespan attributable to heart failure accompanied by severe arteriosclerosis.[8] This makes it difficult to study whether advanced fibrosis or even cirrhosis can be caused solely by HFD feeding. We therefore tried to improve the model and produce NASH with advanced fibrosis, which is more similar to the disease observed in humans that gradually develops after several decades. In the present study, this was accomplished by reducing the concentrations of cholesterol and corn oil in the diet and by prolonging the feeding period from 2 to 9 months.

Supported by the Japan Society for the Promotion of Science (grant-in-aid for scientific research 18659214, 2007, to N.K.) and by a Thrust Area research grant from Osaka City University (2008) (N.K.).

Accepted for publication March 22, 2010.

Portions of this study were presented in abstract form at the 44th Annual Meeting of the European Association for the Study of the Liver, Copenhagen, 2009.

CME Disclosure: None of the authors disclosed any relevant financial relationships.

Supplemental material for this article can be found on *http://ajp.amjpathol.org*.

Address reprint requests to Norifumi Kawada, M.D., Ph.D., Department of Hepatology, Graduate School of Medicine, Osaka City University, 1-4-3, Asahimachi, Abeno, Osaka 545-8585, Japan. E-mail: kawadanori@med.osaka-cu.ac.jp.

NAFLD/NASH is assumed to be most effectively improved by weight control and by restricting lipid and calorie intake, thereby leading to normalized lipid metabolism.[9,10] Nevertheless, drug therapy would be a useful and an easy option because the modern lifestyle habits such as poor diet and lack of regular exercise are difficult to change. Ezetimibe is a relatively new and promising drug candidate for NAFLD/NASH therapy. Ezetimibe selectively inhibits cholesterol absorption via Niemann-Pick C1-like 1 (NPC1L1) protein in the brush border of the small intestine in humans, rodents, rabbits, and other species.[11–15] It decreases the serum levels of low-density lipoprotein cholesterol and triglycerides (TGs) in humans[16] and reduces plaque formation and improves lipids in a rabbit model of atherosclerosis.[17] Recent reports have indicated that ezetimibe improves liver steatosis and insulin resistance in Zucker obese fatty rats[18] and rats fed a methionine- and choline-deficient diet.[19] Thus, ezetimibe is a potential new therapeutic agent for human NASH.[20] In the present study, we also assessed the effect of ezetimibe on the development of NASH in our rabbit model.

Materials and Methods

Materials

Mouse monoclonal antibodies against α-smooth muscle actin (αSMA), rabbit macrophage (clone RAM-11), and 4-hydroxy-2-nonenal (4-HNE) were obtained from Sigma Chemical Co. (St. Louis, MO), Thermo Fisher Scientific (Fremont, CA), and Nikken Seil Co., Ltd. (Shizuoka, Japan), respectively. Enhanced chemiluminescence detection reagent was obtained from Amersham Pharmacia Biotech (Little Chalfont, Buckinghamshire, UK), and Immobilon-P membranes were from Millipore Corp. (Bedford, MA). All other reagents were purchased from Sigma Chemical Co. or Wako Pure Chemical Co. (Osaka, Japan).

Animals and Experimental Protocol

Pathogen-free male Japanese White rabbits, about 1-year-old and weighing 3.0 to 3.5 kg, were obtained from SLC (Shizuoka, Japan). As shown in Figure 1, we performed the following two experiments: i) rabbits were housed at a constant temperature and were given either 100 g/day of a standard diet (SD) (n = 5, CR3 obtained from CLEA Japan Inc., Tokyo, Japan) or version II of an improved high-fat and -cholesterol diet (HFD II) (n = 5), which consisted of SD supplemented with 12% corn oil and 0.75% (w/w) cholesterol for 9 months; and ii) rabbits were given version I (100 g/day) of a previously reported HFD (HFD I), which consisted of SD supplemented with 20% corn oil and 1.25% (w/w) cholesterol for 2 months.[7] The treated group additionally received 0.6 mg/kg/day of ezetimibe mixed in the diet. Ezetimibe was kindly provided by Bayer AG (Leverkusen, Germany). The contents of the SD and HFD I and II are shown in Supplemental Table S1 (see *http://ajp.amjpathol.org*).

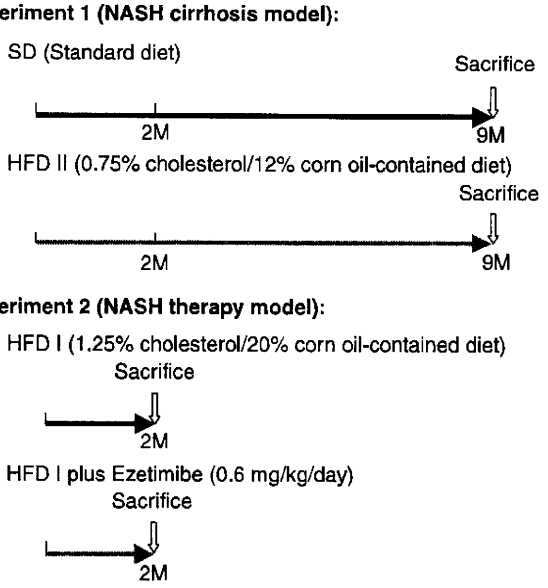

Figure 1. Experimental schedule of the present study. Experiment 1: NASH cirrhosis was induced in rabbits by feeding HFD II for nine months. Experiment 2: during NASH therapy, rabbits were administrated ezetimibe (0.6 mg/kg/day) supplemented with HFD I for two months. In the NASH therapy model, a previously reported HFD I was used to evaluate the effect of medicine during a short period.

The rabbits were fasted 24 hours before sacrifice. Then they were anesthetized and laparotomized for blood and liver sampling. The portal vein was cannulated using an 18-gauge Teflon catheter. The liver of each animal was perfused with 100 ml of PBS to remove the blood. After harvest, the liver was cut into small pieces and fixed in 4% paraformaldehyde. Each sample was either frozen or embedded in paraffin. The experiments were conducted humanely in accordance with the recommendations of the Guide for the Care and Use of Laboratory Animals of Osaka City University School of Medicine.

Histochemical and Immunohistochemical Studies

Paraformaldehyde-fixed specimens were sectioned into 5-μm-thick sections and stained with H&E and 0.1% (w/v) Sirius red (Direct Red 80, Aldrich, Milwaukee, WI). Frozen sections (5-μm-thick) were stained with Oil red O (Wako Pure Chemical Co.). The areas stained by Sirius red and Oil red O were measured to assess the areas of connective tissue and lipid deposition, respectively, using an image analyzer (Lumina Vision, Mitani Corporation, Tokyo, Japan).

Immunohistochemical analysis was performed as described elsewhere.[7] In brief, sections were deparaffinized, washed, and preincubated in 5% bovine serum albumin blocking solution, followed by overnight incubation at 4°C with antibodies against either αSMA at a dilution of 1:100, rabbit macrophage (RAM-11)[21] at a dilution of 1:100, or 4-HNE at a concentration of 5 μg/ml.[22] The sections were incubated with biotinylated sec-

ondary antibodies and reacted with horseradish peroxidase-conjugated streptavidin (Nichirei Biosciences Inc., Tokyo, Japan) and then treated with diaminobenzidine (DAKO, Glostrup, Denmark) for color development.

Laboratory Tests

Serum levels of aspartate aminotransferase (AST), alanine aminotransferase (ALT), total cholesterol (T-Cho), TG, free fatty acid (FFA), and fasting glucose were measured at the Special Reference Laboratories (Osaka, Japan). Fractionation of serum cholesterol was performed by high-performance liquid chromatography at Skylight Biotech (Akita, Japan). The serum and urine levels of oxidative stress markers and antioxidants were measured at Nikken Seil Co., Ltd. Fasting serum insulin levels were measured using a rat insulin enzyme-linked immunosorbent assay kit and a rabbit insulin standard solution (Shibayagi Co. Ltd., Gunma, Japan). Homeostasis model assessment of insulin resistance (HOMA-IR) was calculated using the formula HOMA-IR = [fasting insulin (ng/ml) × 23.1] × fasting glucose (mg/dl)/405. Serum bile acid was measured using a Total Bile Acids Test Wako (Wako Pure Chemical Co.) according to the manufacturer's instructions.

Assay of Hepatic Total Cholesterol, Triglyceride, and Free Fatty Acid Levels

Liver tissue (50 to 100 mg) was homogenized in 0.75 ml of methanol and chloroform (2:1), and lipids were extracted from the chloroform fraction. Then, the hepatic tissue levels of T-Cho and TG were determined using a Cholesterol E-Test Wako and Triglyceride E-Test Wako (Wako Pure Chemical Co.) according to the manufacturer's instructions. The data were expressed as the amount of T-Cho (mg) or TG (mg)/liver wet weight (g).

For the hepatic FFA assay, liver tissue (10 mg) was homogenized in 0.2 ml of chloroform and 1% Triton X-100. Fatty acids were extracted in the chloroform fraction and air-dried to remove the chloroform. Then, the hepatic tissue FFA levels were determined using a Free Fatty Acid Quantification Kit (BioVision, Mountain View, CA) according to the manufacturer's instructions. The data were expressed as the amount of FFA (nmol)/liver wet weight (mg).

Quantitative Real-Time PCR

Total RNA was extracted from the liver using Isogen (Nippon Gene Co. Ltd., Tokyo, Japan). cDNAs were synthesized with 1 μg of total RNA, ReverTra Ace (Toyobo, Osaka, Japan), and oligo(dT)$_{12-18}$ primers according to the manufacturer's instructions.[23] Gene expression was measured by real-time PCR on an Applied Biosystems Prism 7500 system (Applied Biosystems, Foster City, CA) using cDNA, real-time PCR Master Mix Reagents (Toyobo), a set of gene-specific oligonucleotide primers, and the TaqMan probes listed in Table 1.

Immunoblotting

Protein samples (10 μg) were subjected to SDS-polyacrylamide gel electrophoresis (PAGE) and then transferred to Immobilon-P membranes. After blocking, the membranes were treated with the primary antibodies and then with horseradish peroxidase-conjugated secondary antibodies. Immunoreactive bands were visualized using the enhanced chemiluminescence system and documented with LAS 1000 (Fuji Photo Film, Kanagawa, Japan). The density of each band was analyzed using a GS-700 densitometer (Bio-Rad Laboratories, Hercules, CA).[23]

Assay of Hepatic 8-Hydroxy-2′-Deoxyguanosine Levels

Liver tissue (100 to 200 mg) was homogenized in lysis buffer, and hepatic DNA was extracted using the DNA Extractor TIS kit (Wako Pure Chemical Co.). After the DNA was hydrolyzed, 8-hydroxy-2′-deoxyguanosine levels in the liver were measured using a highly sensitive 8-hydroxy-2′-deoxyguanosine enzyme-linked immunosorbent assay kit (Nikken Seil Co. Ltd.) according to the manufacturer's instructions.

Proteome Analysis

Two-dimensional SDS-PAGE was performed by Towa Environment Science (Osaka, Japan).[24] Proteins (100 μg) extracted from rabbit livers were applied to Immobiline DryStrips (pH 3 to 10). After isoelectric focusing, the proteins were separated by SDS-PAGE on 9 to 18 acrylamide gradient gels, visualized by SYPRO Ruby staining, scanned, and analyzed as described previously.[25] Protein spots of interest were excised from the gels, digested in trypsin solution, dialyzed, and then analyzed by electrospray ionization mass spectrometry. The proteins were identified from the obtained amino acid sequences using databases such as protein BLAST or FASTA.

Microarray Analysis

Total RNA was extracted from liver tissues with Isogen. Rabbit microarray chips were designed on the eArray system (Agilent Technologies, Palo Alto, CA) and were provided by Takara Bio Inc. (Shiga, Japan). The gene expression profile of HFD II-fed rabbits was compared with that of SD-fed rabbits. Genes showing differences in expression with an increase of more than fivefold or a decrease to <0.5-fold were recognized as up- or down-regulated genes, respectively, and were targeted for further analysis. The data are partially shown in Supplemental Table S2 (see *http://ajp.amjpathol.org*).

Statistical Analysis

Bar graphs present data as means ± SD of at least three independent experiments. Statistical analysis was per-

Table 1. List of Primer Sequences

Gene	Sequence	Accession no.
PPARγ		
Forward	5′-CCTGGCTTTGTGAGCCTTGAC-3′	AY166780
Reverse	5′-GAGGCCAGCATGGTGTAGATGA-3′	
aP2		
Forward	5′-CAGATGACAGGAAAGGCAAGAGT-3′	AF136241
Reverse	5′-CCTCCCGTTTTCTCTTTATGGT-3′	
LXRα		
Forward	5′-GGAGACGTCTCGCAGGTACA-3′	
Reverse	5′-CCCTGCTTTGGCAAAGTCCT-3′	
SREBP1		
Forward	5′-GACACAGGAGCCACAATGAAGAC-3′	AF278696
Reverse	5′-GCAGTTTGTCTGTGTCCACAACC-3′	
SREBP2		
Forward	5′-GGCGGACAAGACACAATATCA-3′	AF278693
Reverse	5′-GTCCCCATGACCAAGTCTTTCA-3′	
HMGCR		
Forward	5′-TGCTGTGAGAACGTGATTGGG-3′	
Reverse	5′-CTTTCCATCCAAGCAGAGAGGT-3′	
LDLR		
Forward	5′-ACAACCCGGTCTACCAGAAG-3′	M11501
Reverse	5′-ATCTGTCTCGAGGGGTAGGT-3′	
CYP7A1		
Forward	5′-CGATGCCTTGATTTCCCTCACAG-3′	NM_001170929
Reverse	5′-TTGGTTCAGGACGTCTCAAGGTAAG-3′	
G6Pase		
Forward	5′-GCAGGTGTGTACTACGTGATGGT-3′	EU520488
Reverse	5′-GTCAAGCACCGAAATCTGTAGGTC-3′	
PEPCK		
Forward	5′-CACATCCCAACTCTCGCTTCTG-3′	EF616471
Reverse	5′-TCCAAAGATGATGGCATCAATGGG-3′	
TNFα		
Forward	5′-GTCACCCTCAGATCAGCTTCTC-3′	NM_001082263
Reverse	5′-GTTCGCACGCTGGCTCAG-3′	
Probe	5′-CCTGAGTGACAAGCCTCTAGCCCACG-3′	
IL-1β		
Forward	5′-GCCTGAGAACTTTCTTTTCCTTAATC-3′	M26295
Reverse	5′-GATCGTACTGCATCACACTCAAG-3′	
Probe	5′-AAGAACCCGTCCTCTGCAACACCTGG-3′	
IL-10		
Forward	5′-CCTTGTCGGAGATGATCCAGTT-3′	DQ437508
Reverse	5′-ATGGCTGGACTGTGGTTCTCA-3′	
IL-18		
Forward	5′-GCAACCTGTGTTTGAGGATATGC-3′	NM_001122940
Reverse	5′-CCATGCCTCTAGTATTGCTGTCTT-3′	
TLR2		
Forward	5′-TCTGCACAAGCGGGACTTT-3′	NM_001082781
Reverse	5′-TTCTCGATGCAGTCGATGATGT-3′	
TLR4		
Forward	5′-AGCCATGCGGGTATCATTTT-3′	NM_001082732
Reverse	5′-TCCTGCTGAGAAGGCGATACA-3′	
CD14		
Forward	5′-GCGCTAAACTCCCTCAATCTATC-3′	M90488
Reverse	5′-GCCCTATTCAGCTTGTTGCA-3′	
MD2		
Forward	5′-GAAGGGAGAGACTGTGAATACAACAG-3′	NM_001082787
Reverse	5′-GCTATGGCTTCTACAACACATCTG-3′	
HO-1		
Forward	5′-GGAGAACGCCGAGTTCATGA-3′	AY421756
Reverse	5′-GGCCATCACCAGCTTAAAACC-3′	
Probe	5′-AACTTTCAGAAGGGCCAGGTGACTGCC-3′	
TGFβ1		
Forward	5′-AAGGGCTACCACGCCAACTT-3′	AF000133
Reverse	5′-CGGGTTGTGCTGGTTGTACA-3′	
Probe	5′-TGCCTGGGACCCTGCCCCTAC-3′	
Col1A1		
Forward	5′-ACTGGATTGACCCCAACCA-3′	AY633663
Reverse	5′-TTGCCCCAGTGTCCATGTC-3′	
Probe	5′-CTGCAACCTGGATGCCATCAAGGTC-3′	

(*table continues*)

Table 1. *Continued*

Gene	Sequence	Accession no.
Col3A1		
Forward	5′-CATTGGCCCTGTTTGCTTTT-3′	S83371
Reverse	5′-GTTGGTCACTTGTACTGGTTGACA-3′	
MMP-2		
Forward	5′-TCACTCCTGAGATCTGCACACA-3′	NM_001082209
Reverse	5′-CAAATGAACCGGTCCTTGAAG-3′	
MMP-9		
Forward	5′-GCTCCGGTGGATCAGATGTT-3′	NM_001082203
Reverse	5′-AAGCGGTCCTGGCAGAAGT-3′	
Probe	5′-CACACGACGTCTTCCAGTACCGAGAG-3′	
TIMP-1		
Forward	5′-TGGAAAGTGTCTGCGGGTACT-3′	AY829730
Reverse	5′-TTGTCCAGCGATGAGAAACTC-3′	
TIMP-2		
Forward	5′-TCACGCTCTGTGACTTCATCGT-3′	AF069713
Reverse	5′-TGTGGTTCAGGCTCTTCTTCTG-3′	
Probe	5′-CCCTGGGACTCCCTGAGCAGCA-3′	
GPO		
Forward	5′-AAGGTGCTGCTCATTGAGAATG-3′	NM_001085444
Reverse	5′-TTCTCCTGATGCCCAAACTG-3′	
GST		
Forward	5′-CAAGTGGCTGAGTGAGAAGTTCA-3′	NM_001082252
Reverse	5′-TTGCTCTGCGTGAGCTTGT-3′	
Cu,Zn-SOD		
Forward	5′-TGGTGGTCCACGAGAAAGAAG-3′	L12405
Reverse	5′-CGTTCCCGGTCTTTGTACTCT-3′	
Mn-SOD		
Forward	5′-ATTGCTGCGTGTGCGAATC-3′	L28808
Reverse	5′-TCAATCCCCAGCAGTGGAA-3′	
MAT1A		
Forward	5′-TCCACCTGGACAGAAACGAAGAGGA-3′	
Reverse	5′-TCTCGTCAGTGGCATAGCCGAACA-3′	
GNMT		
Forward	5′-AGGGCTTCAGTGTGACGAGTGT-3′	D13307
Reverse	5′-CGGTTCCAGCGCTCTTTAA-3′	
ST3A1		
Forward	5′-GTGCCCTTCTTGGAATACAACA-3′	NM_001082210
Reverse	5′-TGGAAGGTGGGAAGCAAAG-3′	
GAPDH		
Forward	5′-GCCAAAAGGGTCATCATCTCA-3′	AB231852
Reverse	5′-GTGGTTCACGCCCATCACA-3′	
Probe	5′-CCTCCGCCGATGCCCCCA-3′	

formed with Student's *t*-test, and differences were considered significant at $P < 0.05$.

Results

Hepatic Lipid Deposition in Rabbits Fed High-Fat and -Cholesterol Diet II

Rabbits fed HFD I for 2 months exhibited insulin resistance, hepatic steatosis, inflammation, oxidative stress, and mild fibrosis, thus, showing similarity to human NASH as we reported previously.[7] After the feeding period was increased by reducing the fat and cholesterol content in the diet to 60% of the previous level (HFD II) to prolong rabbit survival, we were able to create a model with advanced hepatic fibrosis that was close to cirrhosis. As shown in Table 2, serum T-Cho and TG levels of rabbits fed HFD II for 9 months increased significantly compared with the levels in rabbits fed SD. The serum cholesterol was mainly very low-density lipoprotein and lipoprotein cholesterol according to the high-performance liquid chromatography analysis. However, serum AST and ALT levels in HFD II-fed rabbits did not change significantly compared with those in SD-fed rabbits. Fasting glucose and insulin values in HFD II-fed rabbits were lower than those in SD-fed rabbits, and HOMA-IR was reduced in HFD-fed rabbits.

The livers of HFD II-fed rabbits were enlarged and whitish with an irregular, partially nodular surface (Figure 2, A and B), showing an appearance that was totally different from the livers of SD-fed rabbits. H&E staining indicated degeneration of hepatocytes predominantly around the central vein area (Figure 2, C and D). At a higher magnification, H&E staining also revealed glassy degeneration of hepatocytes, which was similar to the ballooning of hepatocytes in human NASH, fibrosis, and bile duct proliferation (Figure 2, E and F), as well as atheroma in the aorta (Figure 2, G and H). The hepatocytes were strongly positive for Oil red O staining (Figure 3, A and B), Furthermore, hepatic T-Cho content in-

Table 2. Liver Enzymes and Lipid Profile in Serum

Enzymes/lipids	SD	HFD II	*P* value
AST (IU/L)	43.4 ± 29.9	29.3 ± 22.4	NS
ALT (IU/L)	45.6 ± 36.6	19.7 ± 18.2	NS
Cholesterol (mg/dl)			
Total	19.2 ± 3.8	1161.3 ± 406.5	$P < 0.01$
Chylomicron	0.2 ± 0.2	159.6 ± 161.8	NS
Very low-density lipoprotein	1.7 ± 0.6	733.0 ± 294.6	$P < 0.01$
Low-density lipoprotein	2.7 ± 0.8	241.6 ± 74.5	$P < 0.01$
High-density lipoprotein	14.6 ± 4.2	27.1 ± 12.5	NS
TG (mg/dl)	26.7 ± 11.9	205.5 ± 96.3	$P < 0.01$
FFA (μEq/L)	279.7 ± 150.7	168.4 ± 107.9	NS
Fasting glucose (mg/dl)	132.7 ± 11.0	98.4 ± 47.3	$P < 0.05$
Fasting insulin (ng/ml)	1.1 ± 0.2	0.7 ± 0.2	$P < 0.05$
HOMA-IR	8.4 ± 2.3	5.2 ± 2.6	$P < 0.05$
Bile acid	5.3 ± 1.3	33.7 ± 17.4	$P < 0.05$

NS, not significant.

creased significantly in HFD II-fed rabbits (38.3 ± 21.5 μg/mg liver weight) compared with that in SD-fed rabbits (1.5 ± 0.2 μg/mg liver weight), although the hepatic TG and FFA contents were similar (Figure 3C), indicating that mainly cholesterol had accumulated in the hepatocytes of rabbits fed HFD II. Expression of genes related to fat metabolism, such as peroxisome proliferator-activated receptor-γ (PPARγ) and adipocyte lipid-binding protein (aP2), also known as fatty acid binding protein 4, increased

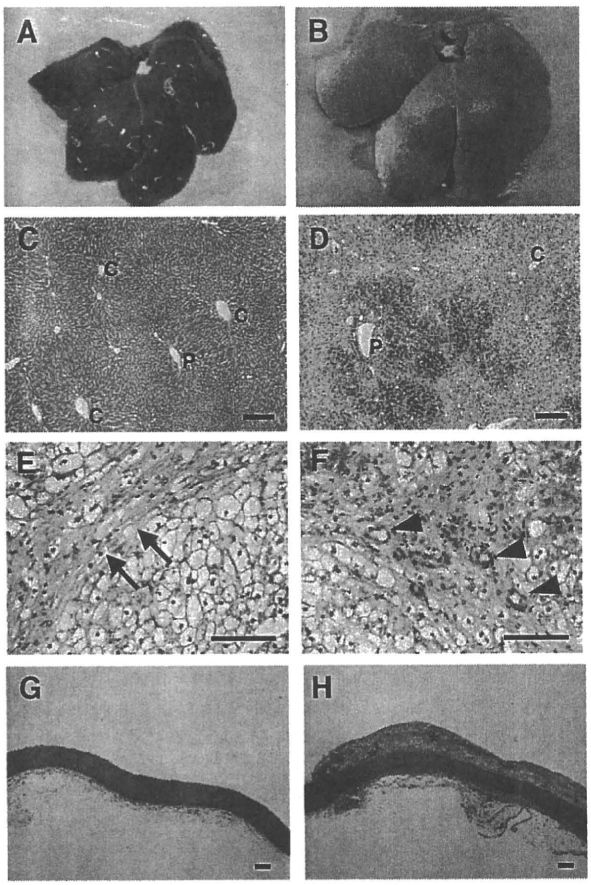

Figure 2. Steatosis and fibrosis in the liver of HFD II-fed rabbits. Rabbits were fed SD (**A**, **C**, and **G**) or HFD II (**B**, **D**, **E**, **F**, and **H**) for nine months. **A** and **B:** Macroscopic appearance of the livers of SD- and HFD II-fed rabbits. **C–H:** H&E staining of the liver (**C–F**) and aorta (**G** and **H**). Note that lipid-induced hepatic degeneration and liver fibrosis are predominantly seen in the livers (**D–F**) and that atheroma developed in the aorta (**H**) of HFD II-fed rabbits. **Arrows** in **E**, **arrowheads** in **F**, and **asterisk** in **H** indicate fibrotic septa, bile duct proliferation, and atheroma, respectively. P, portal vein; C, central vein. Scale bars = 100 μm.

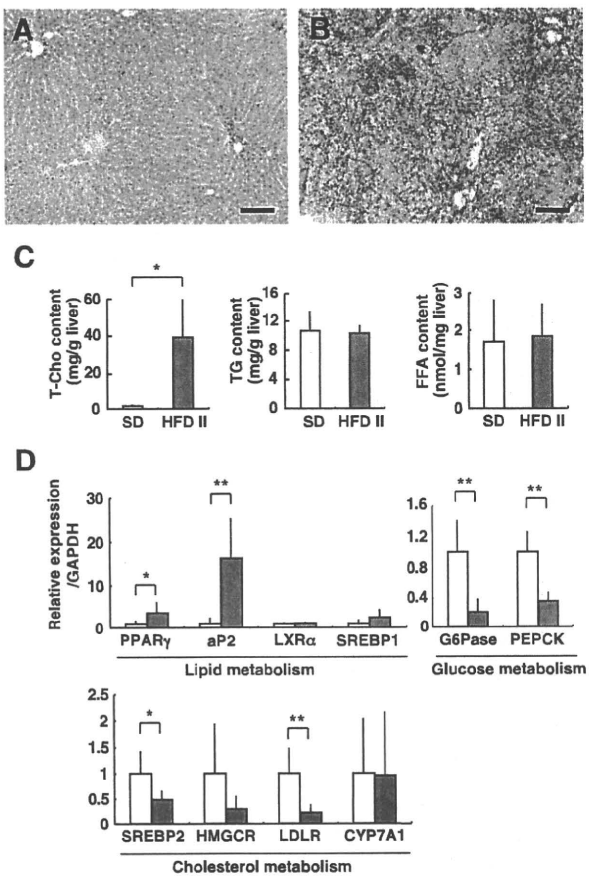

Figure 3. Metabolism of lipid, glucose, and cholesterol in the livers of HFD II-fed rabbits. Rabbits were fed SD (**A**) or HFD II (**B**) for nine months. **A** and **B:** Oil red O staining. Note hepatic lipid deposits in HFD II-fed rabbits. Scale bars = 100 μm. **C:** Hepatic T-Cho (**left**), TG (**middle**), and FFA (**right**) contents. Note that the hepatic T-Cho content increased significantly in HFD II-fed rabbits. **D:** Expression of lipid, glucose, and cholesterol metabolism-related genes in the livers of SD-fed rabbits (white bars) and HFD II-fed rabbits (gray bars) analyzed by quantitative real-time PCR. $^{*}P < 0.05$; $^{**}P < 0.01$.

in rabbits fed HFD II, whereas glucose 6-phosphatase (G6Pase) and phosphoenolpyruvate carboxykinase (PEPCK), which are involved in glucose metabolism, were reduced in the livers of HFD II-fed rabbits (Figure 3D). Among cholesterol biosynthesis-related genes, expression of sterol regulatory element binding protein 2 (SREBP2) and low-density lipoprotein receptor (LDLR) was significantly reduced in the livers of HFD II-fed rabbits. Expression of 3-hydroxy-3-methylglutaryl-coenzyme A reductase (HMGCR) mRNA also tended to be reduced in livers, although not significantly. Cytochrome P450 7A1 (CYP7A1) mRNA levels remained unchanged.

Hepatic Inflammation and Kupffer Cell Activation

RAM-11, an antibody directed against rabbit macrophages, recognizes activated Kupffer cells, the resident liver macrophages.[21] In contrast to the livers of SD-fed rabbits (Figure 4A), in the livers of HFD II-fed rabbits, the number of RAM-11-positive (RAM-11$^+$) cells increased drastically around the central vein area at sites where fatty degeneration of hepatocytes was evident (Figure 4B, see also Figure 2D). At a higher magnification (Figure 4B, inset), large RAM-11$^+$ cells were localized in sinusoids, and they frequently contained vacuoles. In accordance with this observation, genes related to macrophage activation and cytokines, such as tumor necrosis factor α (TNFα); interleukin-1β (IL-1β), -10 (IL10), and -18 (IL18); Toll-like receptors 2 (TLR2) and 4 (TLR4); CD14 (a coreceptor with TLR 4); and MD2 (a complex with TLR4), were all induced in the livers of HFD II-fed rabbits (Figure 4C, Supplemental Table S2, see *http://ajp.amjpathol.org*).

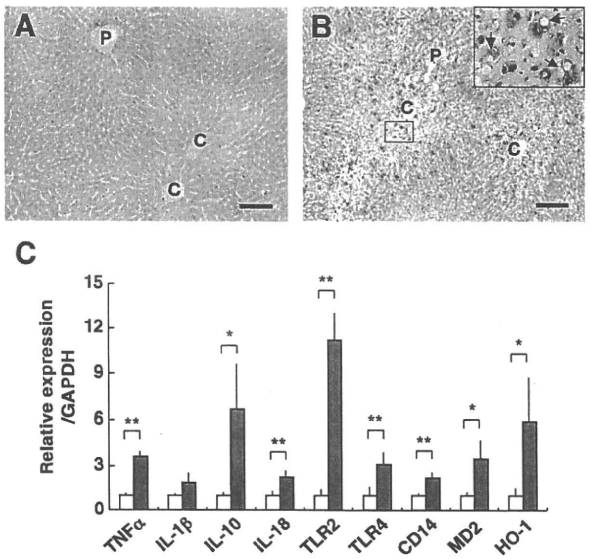

Figure 4. Activation of macrophages in the livers of HFD II-fed rabbits. Rabbits were fed SD (**A**) or HFD II (**B**) for nine months. **A** and **B:** Immunohistochemistry for the rabbit macrophage RAM-11 clone. Note RAM-11$^+$ cells around the central vein area in HFD II-fed rabbits, whereas these cells are absent in SD-fed rabbits. **Inset:** enlarged view of the box. **Arrows** indicate RAM-11$^+$ cells with large vacuoles. Scale bars = 100 μm. P, portal vein; C, central vein. **C:** Expression of inflammatory genes in the livers of SD-fed rabbits (white bars) and HFD II-fed rabbits (gray bars) analyzed by quantitative real-time PCR. $^*P < 0.05$; $^{**}P < 0.01$.

A stress protein, heme oxygenase-1 (*HO-1*), was also increased significantly in the livers of HFD II-fed rabbits.

Advanced Hepatic Fibrosis in Rabbits Fed High-Fat and -Cholesterol Diet II

The livers of HFD II-fed rabbits showed evidence of advanced fibrosis. Sirius red staining showed a limited amount of red-colored collagen around portal and central veins in the control livers, whereas collagen deposition was marked in the livers of HFD II-fed rabbits (Figure 5, A and B). Fibrosis formed bridges between the central veins and central portal veins, indicating that the liver fibrosis was stage 3 (bridging fibrosis) or stage 4 (cirrhosis) according to the Brunt's staging score. The fibrotic septa were composed of cells positive for αSMA, a marker of activated stellate cells and myofibroblasts (Figure 5, C and D). Up-regulated expression of αSMA in HFD II-fed rabbits was confirmed by immunoblotting (Figure 5E). In addition, expression of genes associated with fibrosis, such as transforming growth factor β1 (TGFβ1), collagens 1A1 (Col1A1) and 3A1 (Col3A1), matrix metalloproteinases-2 (MMP-2) and -9 (MMP-9), and tissue inhibitors of metalloproteinases-1 (TIMP-1) and -2 (TIMP-2), increased in the livers of HFD II-fed rabbits (Figure 5F, Supplemental Table S2, see *http://ajp.amjpathol.org*). Furthermore, genes for other matrix proteins such as

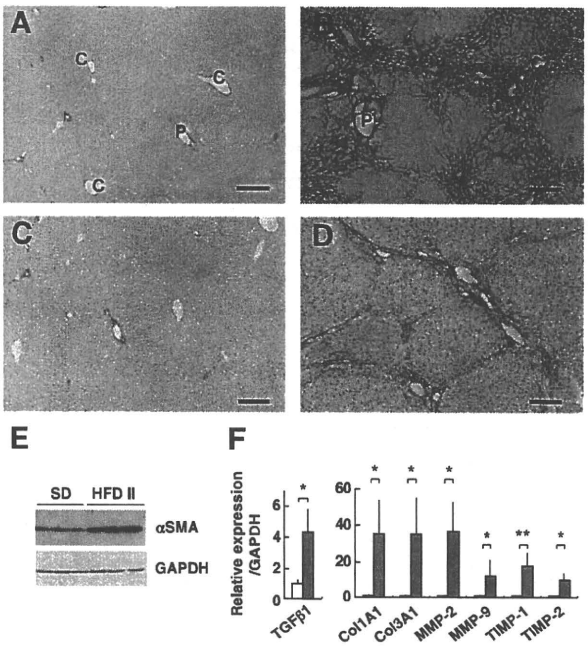

Figure 5. Progression of liver fibrosis in HFD II-fed rabbits. Rabbits were fed SD (**A** and **C**) or HFD II (**B** and **D**) for nine months. **A** and **B:** Sirius red staining. Note collagen deposits around the portal and central vein areas, as well as bridging fibrosis in HFD II-fed rabbits. P, portal vein; C, central vein. **C** and **D:** Immunohistochemistry for αSMA, a marker of activated stellate cells and myofibroblasts. Note that αSMA$^+$ cells are mainly seen inside fibrotic septa in the livers of HFD II-fed rabbits. Scale bar = 100 μm. **E:** Immunoblotting for αSMA. Note that expression of αSMA was augmented in HFD II-fed rabbits. GAPDH was the internal control. **F:** Expression of fibrosis-related genes in the livers of SD-fed rabbits (white bars) and HFD II-fed rabbits (gray bars) analyzed by quantitative real-time PCR. $^*P < 0.05$; $^{**}P < 0.01$.

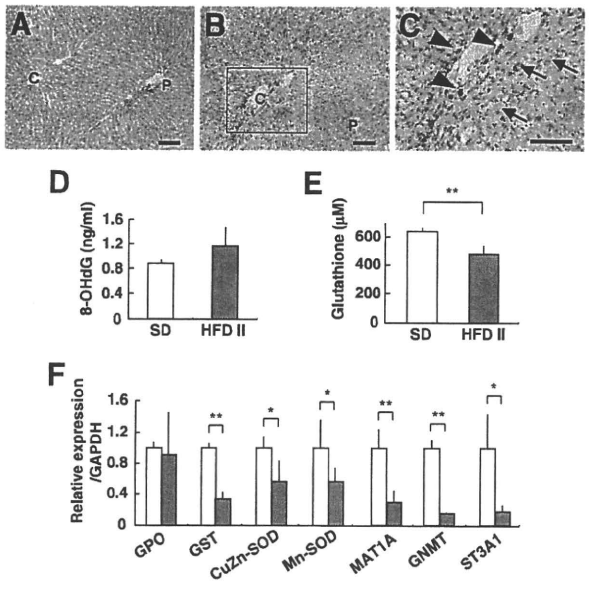

Figure 6. Detection of oxidative stress and levels of antioxidants in the liver. Rabbits were fed SD (**A**) or HFD II (**B** and **C**) for nine months. **A–C:** Staining of 4-HNE adducts in the liver. **C:** A magnified image of the region enclosed within the **box** in **B**. Note 4-HNE adducts in the hepatocytes (**arrows**) and sinusoidal cells (**arrowheads**) of HFD II-fed rabbits. Scale bars = 100 μm. **D:** Hepatic 8-hydroxy-2′-deoxyguanosine content. **E:** Glutathione content in the livers of SD- and HFD II-fed rabbits. **F:** Expression of mRNAs for antioxidant-related genes and proteome analysis of liver proteins in SD-fed rabbits (white bars) and HFD II-fed rabbits (gray bars). $^{*}P < 0.05$; $^{**}P < 0.01$.

collagen 8A1, MMP-12, TIMP-3, lumican, decorin, and biglycan showed increased expression in the livers of HFD II-fed rabbits (Supplemental Table S2, see *http://ajp.amjpathol.org*).

Oxidative Stress and Antioxidant Imbalance in Rabbits Fed High-Fat and -Cholesterol Diet II

Immunohistochemical analysis showed that 4-HNE adduct formation was rare in SD-fed rabbits but was prominent in HFD II-fed rabbits. The 4-HNE adducts were present in the cytoplasm of sinusoidal cells and hepatocytes around the central vein areas (Figure 6, A–C), indicating increased lipid peroxidation in HFD II-fed rabbit livers as in human NASH.[22] Moreover, the 8-hydroxy-2′-deoxyguanosine level increased, although not significantly, in both liver tissue and urine of HFD II-fed rabbits (Figure 6D, Table 3). As a measure of the presence of oxidative stress, the hepatic level of glutathione was determined in SD- and HFD II-fed rabbits; HFD II significantly reduced its levels (Figure 6E). In addition, the expression of genes for glutathione *S*-transferase (GST) and other antioxidant molecules, such as Cu,Zn-superoxide dismutase (Cu,Zn-SOD) and Mn-superoxide dismutase (Mn-SOD), decreased significantly in HFD II-fed rabbits (Figure 6F, Supplemental Table S2, see *http://ajp.amjpathol.org*). We measured the serum or urine levels of molecules that reflect oxidative stress. The levels of copper, δ-tocopherol, and coenzyme Q10 (ubiquinol and ubiquinone) increased significantly in HFD II-fed rabbits, whereas folic acid and vitamin A decreased significantly (Table 3). Comparison of hepatic protein distribution profiles on two-dimensional SDS-PAGE gels between SD- and HFD II-fed rabbits revealed proteins that were both up- and down-regulated by HFD II (Figure 7). GST was identified as a markedly down-regulated protein in HFD II-fed rabbits. Other down-regulated proteins in HFD II-fed rabbits by proteome analysis were glycine *N*-methyltransferase (GNMT), methionine adenosyltransferase 1 (MAT1), and sulfotransferase 3A1 (ST3A1). These genes also showed significantly lower expression in the livers of HFD II-fed rabbits (Figure 6F).

Effect of Ezetimibe on the Rabbit NASH Model

To further evaluate the rabbit NASH model, we investigated the effect of a known compound that suppresses the occurrence of NASH through a known mechanism.

Table 3. Profile of Oxidative Stress Markers and Antioxidants in Serum and Urine

	SD	HFD II	Source	*P* value
Oxidative stress				
8-OHdG (ng/mg creatinine)	43.0 ± 37.7	101.1 ± 34.6	Urine	NS
Isoplastane (ng/mg creatinine)	4.0 ± 5.3	18.2 ± 24.8	Urine	NS
Lipid peroxide (nmol/ml)	2.5 ± 1.0	3.7 ± 0.4	Serum	NS
Antioxidants				
Iron (μg/dl)	142.8 ± 65.7	115.9 ± 24.5	Serum	NS
Copper (μg/dl)	46.8 ± 2.9	156.3 ± 5.9	Serum	$P < 0.01$
STAS (μM)	969.0 ± 39.8	958.7 ± 143.5	Serum	NS
Aqueous antioxidants				
Vitamin C (μg/ml)	3.9 ± 1.3	6.3 ± 2.9	Serum	NS
Folic acid (ng/ml)	55.8 ± 11.6	21.3 ± 12.5	Serum	$P < 0.05$
Liposoluble antioxidants				
Vitamin A (μg/dl)	92.3 ± 5.1	37.6 ± 6.7	Serum	$P < 0.01$
Vitamin E fraction				
α-Tocopherol (μg/dl)	95.0 ± 81.4	3499.7 ± 5040.3	Serum	NS
δ-Tocopherol (μg/dl)	<2.5	31.2 ± 10.4	Serum	$P < 0.05$
γ-Tocopherol (μg/dl)	6.5 ± 2.7	706.9 ± 944.2	Serum	NS
Coenzyme Q10				
Ubiquinol (nmol/L)	58.0 ± 10.8	489.3 ± 151.3	Serum	$P < 0.05$
Ubiquinone (nmol/L)	N.D.	36.7 ± 23.7	Serum	$P < 0.01$

NS, not significant.

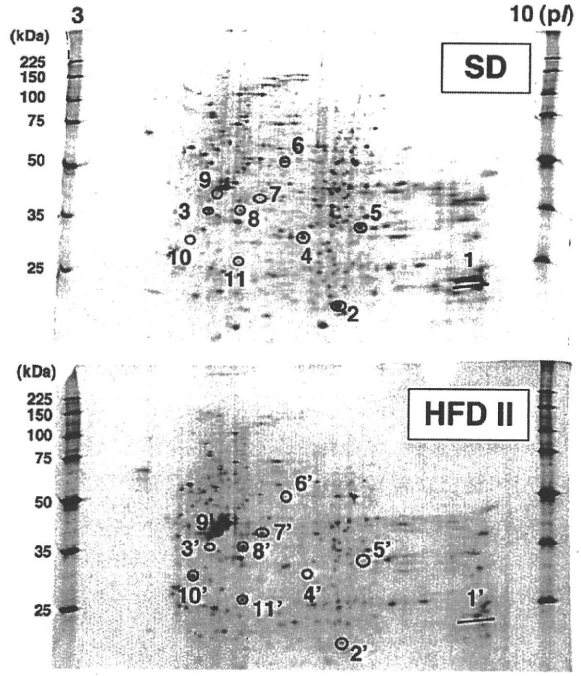

Figure 7. Two-dimensional SDS-PAGE analysis of hepatic proteins. Rabbits were fed SD or HFD II for nine months. Proteins were extracted from the livers of SD- and HFD II-fed rabbits and were separated by two-dimensional SDS-PAGE. After the gels were stained with SYPRO Ruby, the protein spots were cut out, digested, and analyzed by quadrupole time-of-flight. Then, the proteins were identified from the obtained amino acid sequences using protein BLAST or FASTA databases. 1 and 1′, glutathione transferase; 2 and 2′, glutathione *S*-transferase Yc (α II); 3 and 3′, MAT1; 4 and 4′, ST3A1; 5 and 5′, GNMT; 6 and 6′, aldehyde dehydrogenase, mitochondrial (ALDH class 2); 7 and 7′, keratin, type II or cytoskeletal 2 epidermal; 8 and 8′, α-tubulin, actin, β-like 2, or similar to actin, cytoplasmic 1; 9 and 9′, actin, β-like 2; 10 and 10′, keratin 10 or CYP2B3; 11 and 11′, similar to actin, cytoplasmic 1. Blue circles, proteins down-regulated in HFD II-fed rabbits; red circles, proteins up-regulated in HFD II-fed rabbits.

Because a marked increase in serum and hepatic T-Cho levels was evident in our HFD-fed rabbits, we tested ezetimibe, a relatively new compound that inhibits NPC1L1 in hepatocytes and the intestine. Rabbits were fed HFD I (the original diet) with or without ezetimibe (0.6 mg/kg/day) for 2 months. Both control and experimental rabbits showed normal increases in body weight (data not shown). Levels of AST, ALT, and TG remained within the normal range in rabbits fed HFD I with or without ezetimibe (AST, 38.0 ± 18.4 versus 20.8 ± 7.4 IU/L; ALT, 11.0 ± 1.0 versus 7.8 ± 3.0 IU/L; and TG, 31.0 ± 9.5 versus 27.4 ± 16.8 mg/dl). Serum T-Cho was significantly lower in HFD I-fed rabbits treated with ezetimibe than in untreated rabbits during the course of ezetimibe-treatment for up to 8 weeks (Figure 8A). A histological examination showed that ezetimibe suppressed fat deposition (Figure 8, B–F) and reduced the hepatic content of total T-Cho and TG (Figure 8G). Furthermore, liver fibrosis, mildly induced in this 2-month HFD I model, was suppressed by the ezetimibe treatment (Figure 9, A–D). Moreover, ezetimibe significantly decreased the expression of genes associated with liver fibrosis, such as TGFβ1, MMP-9, and TIMP-1 and -2. The drug also suppressed expression of Col1A1 and MMP-2, although the difference was not significant (Figure 9E).

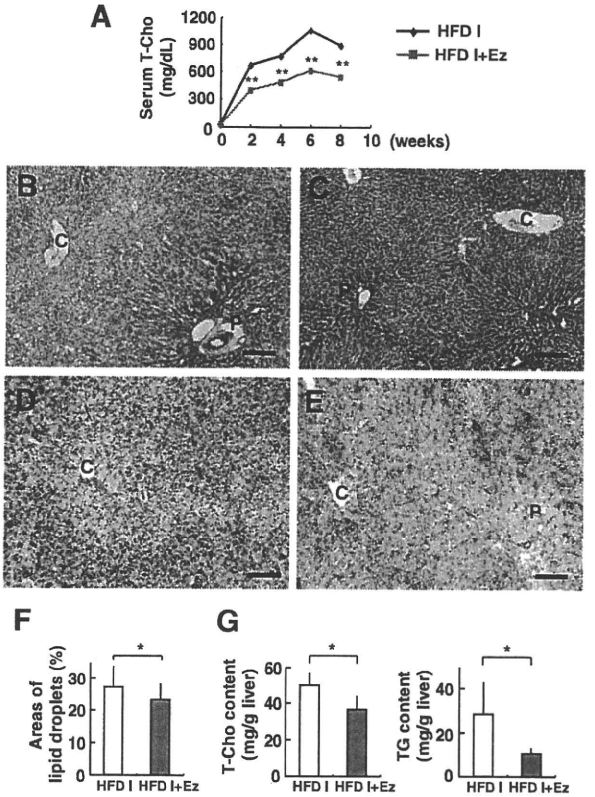

Figure 8. Effect of ezetimibe (Ez) on hepatic steatosis in HFD I-fed rabbits. Rabbits were fed HFD I (the original diet) with or without ezetimibe (0.6 mg/kg/day) (HFD I or HFD I + Ez) for two months. Histological sections were prepared from HFD I-fed (**B** and **D**) and HFD I + Ez-fed rabbits (**C** and **E**). **A:** Changes in serum T-Cho levels. **B** and **C:** H&E staining. **D** and **E:** Oil red O staining. Scale bars = 100 μm. **F:** Quantification of the lipid droplet area in the liver. Oil red O-stained areas were measured in the livers of HFD I- and HFD I + Ez-fed rabbits. The stained area was significantly smaller in HFD I + Ez-fed rabbits. **G:** Hepatic total cholesterol and triglyceride contents. P, portal vein; C, central vein. HFD I, $n = 5$. HFD I + Ez, $n = 5$. $^{*}P < 0.05$; $^{**}P < 0.01$.

Discussion

There are several important differences in characteristics of NASH between this rabbit model and humans. Hepatic levels of cholesterol, but not of TG and FFA, exhibited a marked increase in HFD II-fed rabbits compared with those in SD-fed rabbits, and the PPARγ and aP2 mRNA levels were induced in the HFD II model in a manner similar to that observed in human NASH (Figure 3, C and D).[26,27] NAFLD shows various patterns of lipid deposition in the liver,[28] which may be influenced by the diet composition. In this context, increased PPARγ and aP2 may contribute to a decrease in cholesterol level in hepatocytes of this rabbit model induced by high-cholesterol diets. Mitochondrial free cholesterol, but not TG and FFA, sensitizes hepatocytes to TNFα- and Fas-induced apoptosis through mitochondrial glutathione exhaustion.[29] We also observed a marked reduction in glutathione and glutathione-metabolic enzymes in the HFD II-fed rabbit livers (Figure 6, E and F). In this context, it is likely that cholesterol overload, together with a dysregulated antioxidative system in hepatocytes, may trigger liver injury.[30,31] Furthermore, this rabbit model showed increased levels

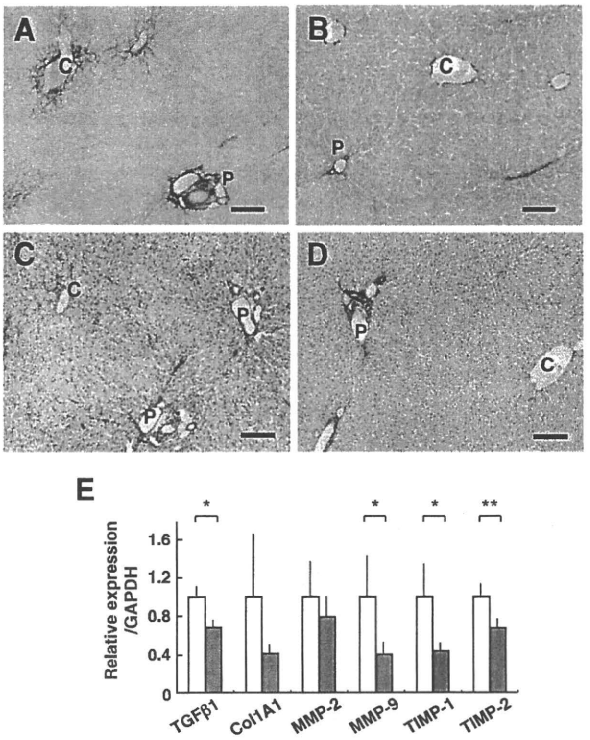

Figure 9. Effect of ezetimibe (Ez) on liver fibrosis in HFD I-fed rabbits. Rabbits were fed HFD I (the original diet) with or without ezetimibe (0.6 mg/kg/day) (HFD I or HFD I + Ez) for two months as mentioned in Figure 8. Histological sections were prepared from HFD I-fed (**A** and **C**) and HFD I + Ez-fed rabbits (**B** and **D**). **A** and **B:** Liver sections were stained with Sirius red. Collagen depositions were reduced by ezetimibe administration. **C** and **D:** Liver sections were immunostained for αSMA. Note that the αSMA^+ cells were reduced by ezetimibe administration. Scale bars = 100 μm. **E:** Expression of fibrosis-related genes in the liver of HFD I-fed rabbits (white bars) and HFD I + Ez-fed rabbits (gray bars). P, portal vein; C, central vein. HFD I, $n = 5$. HFD I + Ez, $n = 5$. Ez, ezetimibe. $^*P < 0.05$; $^{**}P < 0.01$.

of serum bile acids (Table 2), which are presumably induced by cholesterol overload and down-regulation of the bile acid export-related genes, such as the bile salt export pump and multidrug resistance-associated protein 2 (data not shown).

Although it has been reported that FFA and leptin increase and adiponectin decreases in the serum of NASH patients,[32] serum and hepatic levels of FFA did not change in this rabbit model, possibly owing to the lack of obesity. A recent study reported the reduction of serum adiponectin in a rabbit model fed 10% lard and 2% cholesterol-containing HFD for 8 and 12 weeks.[33] Unfortunately, we were unable to determine the adiponectin and leptin levels in our rabbit model for unknown reasons (data not shown).

We also observed no increase in fasting glucose, fasting insulin, or HOMA-IR in this rabbit model. However, as stated above, this rabbit model showed no obesity and failed to induce high FFA levels in the liver and serum, which may be reasons for its failure to induce type II diabetes and insulin resistance. Furthermore, as shown in Figure 3D, G6Pase and PEPCK mRNA expression levels were markedly suppressed in the HFD II model, similar to a report on cirrhotic NASH patients.[34] Cholesterol overload and the resulting hepatocyte dysfunction in cirrhosis are assumed to be the reasons for this down-regulation, indicating the actual impairment of glucose metabolism in the HFD II liver.

The serum ALT level has long been used as a surrogate marker for liver injury. However, ALT values do not correlate well with the severity of liver injury in human NAFLD.[35,36] Similar to that in patients with NAFLD but that inunlike viral or drug-induced hepatitis, the ALT level in this rabbit model remained unchanged, but the mechanism remains unknown and should be clarified in future research.

Gut-derived lipopolysaccharide activates Kupffer cells by activating lipopolysaccharide receptors,[37] leading to increased production of inflammatory cytokines such as TNFα, IL-8, and IL-18.[38,39] The development of steatohepatitis in a NASH model, induced by a methionine- and choline-deficient diet, was partly inhibited in TLR4 mutant mice,[40,41] suggesting a role for TLR4-dependent signaling in the occurrence of this type of liver damage. In addition, the lipoprotein component of endotoxin from Gram-negative and -positive bacteria activates TLR2 and/or TLR4, which leads to common downstream activation of TRAF6 via the adapter molecule MyD88.[42] This cascade of events culminates in nuclear factor-κB activation, leading to the induction of TNFα and other proinflammatory cytokines.[42] Although TNFα has been identified as a central mediator contributing to insulin resistance and liver damage in NASH, little is known about the role of TLR2 or TLR4 in the induction of TNFα. In the present study, we observed an increase in the expression of TLR4/CD14/MD2 and TLR2 and cytokine induction in HFD II-fed rabbits. Persistent hepatic inflammation also triggers the activation of stellate cells and excess collagen production, resulting in the development of liver fibrosis.[43,44] Stellate cells are activated by LPS through TLR4/CD14/MD2 signaling.[45,46] Thus, the role of LPS in triggering steatohepatitis in this HFD II model deserves to be studied further in relation to hepatic fibrogenesis.

In the present study, we showed a reduction in hepatic glutathione content and decreased GST and SOD mRNA expression. Serum levels of antioxidants such as vitamin E, copper, and coenzyme Q10 increased significantly, but the levels of vitamin A and folic acid decreased significantly. As a result, there was an imbalance between oxidative stress and antioxidant protection systems in the present steatohepatitis model, as in human NASH patients.[47–52] The molecular mechanisms leading to the dysregulation of small antioxidant molecules are currently unknown. Most vitamin A in the body (approximately 70%) is usually stored in quiescent hepatic stellate cells,[53] but vitamin A storage is impeded when stellate cells are activated, under which activation they express αSMA and produce extracellular matrix materials including type I collagen.[43,44] Thus, the reduction of serum vitamin A levels may reflect activation of stellate cells and the progression of fibrosis in our rabbits with HFD II-induced NASH. Folic acid is reportedly involved in the maintenance of normal concentrations of homocysteine, methionine, and *S*-adenosylmethionine.[54] Folic acid deficiency and abnormal hepatic methionine metabolism

are characteristics of alcoholic liver disease.[54] Thus, the reduction in serum folic acid observed in our rabbit NASH model might be a common feature of both alcoholic and nonalcoholic liver disease. Furthermore, the proteome analysis identified a reduction in GNMT and MAT1, which are associated with liver steatosis and fibrosis, in HFD II-fed rabbits.[55–57] Martínez-Chantar et al[55] showed that GNMT-knockout mice exhibited an elevation in serum aminotransferase, methionine, and *S*-adenosylmethionine and developed hepatic steatosis, fibrosis, and hepatocellular carcinoma. MAT1A-knockout mice were also reported to show liver steatosis.[57] These enzymes play an important role in the synthesis and degradation of *S*-adenosylmethionine.[56] Thus, an imbalance in *S*-adenosylmethionine and methionine metabolism may play a role in the development of steatohepatitis in our model.[58]

Phagocytic NADPH oxidases, such as gp91-phox, p40-phox, p67-phox, and p22-phox, increased in the present rabbit model (Supplemental Table S2, see *http://ajp.amjpathol.org*); however, the role of NADPH oxidase, a key molecule in the development of atherosclerosis,[59] in NASH is poorly understood. In alcoholic liver injury, NADPH oxidase is important for reactive oxygen species production in Kupffer cells and in hepatic stellate cells that initiate and promote liver injury.[60,61] We previously reported that the phagocytic activity of Kupffer cells promotes oxidative stress, inflammation, and fibrosis in steatohepatitis.[7] In this context, NADPH oxidase could play a prominent role in the pathogenesis of human NASH.

In the present study, we created a rabbit model of steatohepatitis, in which advanced fibrosis (close to cirrhosis) was produced by feeding a HFD. Hypercholesterolemia is a risk factor for liver injury as well as for atherosclerosis;[2–5] therefore, lowering the serum T-Cho level by dieting or by medications that reduce the synthesis and absorption of cholesterol could be a promising therapy for NAFLD including NASH. In this context, statins, which are HMG-CoA reductase inhibitors, have been reported to improve NASH.[62,63] Rallidis et al[62] showed that pravastatin treatment lowered serum ALT and improved histological steatosis in 5 NASH patients. Hyogo et al[63] treated patients with atorvastatin and found that 23 patients (74.2%) exhibited normalized transaminases and histological improvement of liver steatosis and the NAFLD activity score, and these changes were accompanied by a significant increase in serum adiponectin and a significant decrease in serum TNFα. In the present study, we studied the effect of ezetimibe, which inhibits NPC1L1 and therefore blocks intestinal absorption of cholesterol from the diet or that excreted in the bile.[11–15] The effect of ezetimibe on NASH has already been reported in rat models. Assy et al[19] studied methionine and choline deficiency-induced steatohepatitis in rats, in which ezetimibe administration alone or together with rosiglitazone, metformin, and valsartan reduced the hepatic levels of TG, T-Cho, and malondialdehyde and also significantly attenuated histological steatosis. In Zucker obese fatty rats, Deushi et al[18] reported that ezetimibe administration reduced the serum and hepatic levels of T-Cho and TG, the number of Oil red O-positive hepatocytes, Sirius red-stained collagen deposition, and αSMA expression. Supporting these observations, we demonstrated the usefulness of ezetimibe treatment in a rabbit NASH model. Because human lipid metabolism is similar to that of rabbits but is different from that of mice and rats, our results strengthen the potential of ezetimibe for controlling fat deposition and fibrosis in human NASH. Interestingly, ezetimibe not only improved HFD I-induced liver steatosis but also reduced fibrosis and the number of αSMA$^+$ cells. In chronic liver disease, TGFβ1 plays an important role in the progression of liver fibrosis and stellate cell activation.[43,44] TGFβ1 produced by Kupffer cells and stellate cells activates stellate cells in a paracrine as well as an autocrine manner and stimulates type I collagen production. In our rabbit model, ezetimibe reduced TGFβ1 and type I collagen expression in the liver. Unlike mice, humans and rabbits show abundant NPC1L1 expression in the liver.[15] Further studies are required to clarify the effect of ezetimibe prophylactically after the HFD-fed rabbits have already developed steatohepatitis and to examine whether ezetimibe directly affects cholesterol metabolism in hepatocytes, thereby participating in the local prevention of fibrosis caused by abnormal cholesterol metabolism.[14]

In conclusion, rabbits fed HFD II for 9 months developed steatohepatitis with advanced fibrosis accompanied by the augmented expression of relevant genes. We demonstrated the presence of an imbalance between oxidative stress and antioxidant levels in HFD II-fed rabbits. Ezetimibe therapy was promising for alleviating the pathological changes in this model, suggesting the potential usefulness of this compound for human liver diseases caused by cholesterol overload.

Acknowledgments

We thank Dr. Ryoko Shiga, Dr. Yong-ping Mu, Ms. Mami Mori, Ms. Michiko Ohashi, and Ms. Asuka Yoshida for their technical support.

References

1. Ford ES, Giles WH, Dietz WH: Prevalence of the metabolic syndrome among US adults: findings from the Third National Health and Nutrition Examination Survey. JAMA 2002, 287:356–359
2. Angulo P: Nonalcoholic fatty liver disease. N Engl J Med 2002, 346:1221–1231
3. Ludwig J, Viggiano TR, McGill DB, Oh BJ: Nonalcoholic steatohepatitis: Mayo Clinic experiences with a hitherto unnamed disease. Mayo Clin Proc 1980, 55:434–438
4. Matteoni CA, Younossi ZM, Gramlich T, Boparai N, Liu YC, McCullough AJ: Nonalcoholic fatty liver disease: a spectrum of clinical and pathological severity. Gastroenterology 1999, 116:1413–1419
5. Brunt EM, Janney CG, Di Bisceglie AM, Neuschwander-Tetri BA, Bacon BR: Nonalcoholic steatohepatitis: a proposal for grading and staging the histological lesions. Am J Gastroenterol 1999, 94:2467–2474
6. Neuschwander-Tetri BA, Caldwell SH: Nonalcoholic steatohepatitis: summary of an AASLD Single Topic Conference. Hepatology 2003, 37:1202–1219
7. Otogawa K, Kinoshita K, Fujii H, Sakabe M, Shiga R, Nakatani K, Ikeda K, Nakajima Y, Ikura Y, Ueda M, Arakawa T, Hato F, Kawada N: Erythrophagocytosis by liver macrophages (Kupffer cells) promotes oxidative stress, inflammation, and fibrosis in a rabbit model of

steatohepatitis: implications for the pathogenesis of human nonalcoholic steatohepatitis. Am J Pathol 2007, 170:967–980
8. Buja LM, Kita T, Goldstein JL, Watanabe Y, Brown MS: Cellular pathology of progressive atherosclerosis in the WHHL rabbit. An animal model of familial hypercholesterolemia. Arteriosclerosis 1983, 3:87–101
9. Okita M, Hayashi M, Sasagawa T, Takagi K, Suzuki K, Kinoyama S, Ito T, Yamada G: Effect of a moderately energy-restricted diet on obese patients with fatty liver. Nutrition 2001, 17:542–547
10. Huang MA, Greenson JK, Chao C, Anderson L, Peterman D, Jacobson J, Emick D, Lok AS, Conjeevaram HS: One-year intense nutritional counseling results in histological improvement in patients with non-alcoholic steatohepatitis: a pilot study. Am J Gastroenterol 2005, 100:1072–1081
11. Altmann SW, Davis HR Jr, Zhu LJ, Yao X, Hoos LM, Tetzloff G, Iyer SP, Maguire M, Golovko A, Zeng M, Wang L, Murgolo N, Graziano MP: Niemann-Pick C1 like 1 protein is critical for intestinal cholesterol absorption. Science 2004, 303:1201–1204
12. Davis HR Jr, Zhu LJ, Hoos LM, Tetzloff G, Maguire M, Liu J, Yao X, Iyer SP, Lam MH, Lund EG, Detmers PA, Graziano MP, Altmann SW: Niemann-Pick C1 like 1 (NPC1L1) is the intestinal phytosterol and cholesterol transporter and a key modulator of whole-body cholesterol homeostasis. J Biol Chem 2004, 279:33586–33592
13. Temel RE, Tang W, Ma Y, Rudel LL, Willingham MC, Ioannou YA, Davies JP, Nilsson LM, Yu L: Hepatic Niemann-Pick C1-like 1 regulates biliary cholesterol concentration and is a target of ezetimibe. J Clin Invest 2007, 117:1968–1978
14. Ge L, Wang J, Qi W, Miao HH, Cao J, Qu YX, Li BL, Song BL: The cholesterol absorption inhibitor ezetimibe acts by blocking the sterol-induced internalization of NPC1L1. Cell Metab 2008, 7:508–519
15. Hawes BE, O'Neill KA, Yao X, Crona JH, Davis HR Jr, Graziano MP, Altmann SW: In vivo responsiveness to ezetimibe correlates with Niemann-Pick C1 like-1 (NPC1L1) binding affinity: comparison of multiple species NPC1L1 orthologs. Mol Pharmacol 2007, 71:19–29
16. Knopp RH, Dujovne CA, Le Beaut A, Lipka LJ, Suresh R, Veltri EP: Evaluation of the efficacy, safety, and tolerability of ezetimibe in primary hypercholesterolaemia: a pooled analysis from two controlled phase III clinical studies. Int J Clin Pract 2003, 57:363–368
17. Gómez-Garre D, Munoz-Pacheco P, Gonzalez-Rubio ML, Aragoncillo P, Granados R, Fernandez-Cruz A: Ezetimibe reduces plaque inflammation in a rabbit model of atherosclerosis and inhibits monocyte migration in addition to its lipid-lowering effect. Br J Pharmacol 2009, 156:1218–1227
18. Deushi M, Nomura M, Kawakami A, Haraguchi M, Ito M, Okazaki M, Ishii H, Yoshida M: Ezetimibe improves liver steatosis and insulin resistance in obese rat model of metabolic syndrome. FEBS Lett 2007, 581:5664–5670
19. Assy N, Grozovski M, Bersudsky I, Szvalb S, Hussein O: Effect of insulin-sensitizing agents in combination with ezetimibe, and valsartan in rats with non-alcoholic fatty liver disease. World J Gastroenterol 2006, 12:4369–4376
20. Yamagishi S, Nakamura K, Matsui T, Sato T, Takeuchi M: Inhibition of intestinal cholesterol absorption by ezetimibe is a novel therapeutic target for fatty liver. Med Hypotheses 2006, 66:844–846
21. Buyssens N, Kockx MM, Herman AG, Lazou JM, Van den Berg K, Wisse E, Geerts A: Centrolobular liver fibrosis in the hypercholesterolemic rabbit. Hepatology 1996, 24:939–946
22. Seki S, Kitada T, Yamada T, Sakaguchi H, Nakatani K, Wakasa K: In situ detection of lipid peroxidation and oxidative DNA damage in non-alcoholic fatty liver diseases. J Hepatol 2002, 37:56–62
23. Otogawa K, Ogawa T, Shiga R, Nakatani K, Ikeda K, Nakajima Y, Kawada N: Attenuation of acute and chronic liver injury in rats by iron-deficient diet. Am J Physiol Regul Integr Comp Physiol 2008, 294:R311–R320
24. Kawada N, Kristensen DB, Asahina K, Nakatani K, Minamiyama Y, Seki S, Yoshizato K: Characterization of a stellate cell activation-associated protein (STAP) with peroxidase activity found in rat hepatic stellate cells. J Biol Chem 2001, 276:25318–25323
25. Kristensen DB, Kawada N, Imamura K, Miyamoto Y, Tateno C, Seki S, Kuroki T, Yoshizato K: Proteome analysis of rat hepatic stellate cells. Hepatology 2000, 32:268–277
26. Greco D, Kotronen A, Westerbacka J, Puig O, Arkkila P, Kiviluoto T, Laitinen S, Kolak M, Fisher RM, Hamsten A, Auvinen P, Yki-Jarvinen H: Gene expression in human NAFLD. Am J Physiol Gastrointest Liver Physiol 2008, 294:G1281–G1287
27. Nakamuta M, Kohjima M, Morizono S, Kotoh K, Yoshimoto T, Miyagi I, Enjoji M: Evaluation of fatty acid metabolism-related gene expression in nonalcoholic fatty liver disease. Int J Mol Med 2005, 16:631–635
28. Puri P, Baillie RA, Wiest MM, Mirshahi F, Choudhury J, Cheung O, Sargeant C, Contos MJ, Sanyal AJ: A lipidomic analysis of nonalcoholic fatty liver disease. Hepatology 2007, 46:1081–1090
29. Marí M, Caballero F, Colell A, Morales A, Caballeria J, Fernandez A, Enrich C, Fernandez-Checa JC, Garcia-Ruiz C: Mitochondrial free cholesterol loading sensitizes to TNF- and Fas-mediated steatohepatitis. Cell Metab 2006, 4:185–198
30. Begriche K, Igoudjil A, Pessayre D, Fromenty B: Mitochondrial dysfunction in NASH: causes, consequences and possible means to prevent it. Mitochondrion 2006, 6:1–28
31. Parola M, Robino G: Oxidative stress-related molecules and liver fibrosis. J Hepatol 2001, 35:297–306
32. Musso G, Gambino R, Durazzo M, Biroli G, Carello M, Faga E, Pacini G, De Michieli F, Rabbione L, Premoli A, Cassader M, Pagano G: Adipokines in NASH: postprandial lipid metabolism as a link between adiponectin and liver disease. Hepatology 2005, 42:1175–1183
33. Fu JF, Fang YL, Liang L, Wang CL, Hong F, Dong GP: A rabbit model of pediatric nonalcoholic steatohepatitis: the role of adiponectin. World J Gastroenterol 2009, 15:912–918
34. Sreekumar R, Rosado B, Rasmussen D, Charlton M: Hepatic gene expression in histologically progressive nonalcoholic steatohepatitis. Hepatology 2003, 38:244–251
35. Mofrad P, Contos MJ, Haque M, Sargeant C, Fisher RA, Luketic VA, Sterling RK, Shiffman ML, Stravitz RT, Sanyal AJ: Clinical and histologic spectrum of nonalcoholic fatty liver disease associated with normal ALT values. Hepatology 2003, 37:1286–1292
36. Wong VW, Wong GL, Tsang SW, Hui AY, Chan AW, Choi PC, Chim AM, Chu S, Chan FK, Sung JJ, Chan HL: Metabolic and histological features of non-alcoholic fatty liver disease patients with different serum alanine aminotransferase levels. Aliment Pharmacol Ther 2009, 29:387–396
37. Enomoto N, Yamashina S, Kono H, Schemmer P, Rivera CA, Enomoto A, Nishiura T, Nishimura T, Brenner DA, Thurman RG: Development of a new, simple rat model of early alcohol-induced liver injury based on sensitization of Kupffer cells. Hepatology 1999, 29:1680–1689
38. Tomita K, Tamiya G, Ando S, Ohsumi K, Chiyo T, Mizutani A, Kitamura N, Toda K, Kaneko T, Horie Y, Han JY, Kato S, Shimoda M, Oike Y, Tomizawa M, Makino S, Ohkura T, Saito H, Kumagai N, Nagata H, Ishii H, Hibi T: Tumour necrosis factor α signalling through activation of Kupffer cells plays an essential role in liver fibrosis of non-alcoholic steatohepatitis in mice. Gut 2006, 55:415–424
39. Wang HN, Wang YR, Liu GQ, Liu Z, Wu PX, Wei XL, Hong TP: Inhibition of hepatic interleukin-18 production by rosiglitazone in a rat model of nonalcoholic fatty liver disease. World J Gastroenterol 2008, 14:7240–7246
40. Szabo G, Velayudham A, Romics L Jr, Mandrekar P: Modulation of non-alcoholic steatohepatitis by pattern recognition receptors in mice: the role of Toll-like receptors 2 and 4. Alcohol Clin Exp Res 2005, 29:140S–145S
41. Rivera CA, Adegboyega P, van Rooijen N, Tagalicud A, Allman M, Wallace M: Toll-like receptor-4 signaling and Kupffer cells play pivotal roles in the pathogenesis of non-alcoholic steatohepatitis. J Hepatol 2007, 47:571–579
42. Akira S, Takeda K: Toll-like receptor signalling. Nat Rev Immunol 2004, 4:499–511
43. Kawada N: The hepatic perisinusoidal stellate cell. Histol Histopathol 1997, 12:1069–1080
44. Friedman SL: Molecular regulation of hepatic fibrosis, an integrated cellular response to tissue injury. J Biol Chem 2000, 275:2247–2250
45. Paik YH, Schwabe RF, Bataller R, Russo MP, Jobin C, Brenner DA: Toll-like receptor 4 mediates inflammatory signaling by bacterial lipopolysaccharide in human hepatic stellate cells. Hepatology 2003, 37:1043–1055
46. Seki E, De Minicis S, Osterreicher CH, Kluwe J, Osawa Y, Brenner DA, Schwabe RF: TLR4 enhances TGF-β signaling and hepatic fibrosis. Nat Med 2007, 13:1324–1332
47. Koruk M, Taysi S, Savas MC, Yilmaz O, Akcay F, Karakok M: Oxidative stress and enzymatic antioxidant status in patients with nonalcoholic steatohepatitis. Ann Clin Lab Sci 2004, 34:57–62
48. Nobili V, Pastore A, Gaeta LM, Tozzi G, Comparcola D, Sartorelli MR, Marcellini M, Bertini E, Piemonte F: Glutathione metabolism and an-

tioxidant enzymes in patients affected by nonalcoholic steatohepatitis. Clin Chim Acta 2005, 355:105–111
49. Yesilova Z, Yaman H, Oktenli C, Ozcan A, Uygun A, Cakir E, Sanisoglu SY, Erdil A, Ates Y, Aslan M, Musabak U, Erbil MK, Karaeren N, Dagalp K: Systemic markers of lipid peroxidation and antioxidants in patients with nonalcoholic fatty liver disease. Am J Gastroenterol 2005, 100:850–855
50. Chalasani N, Deeg MA, Crabb DW: Systemic levels of lipid peroxidation and its metabolic and dietary correlates in patients with nonalcoholic steatohepatitis. Am J Gastroenterol 2004, 99:1497–1502
51. Akin K, Beyler AR, Kaya M, Erden E: The importance of iron and copper accumulation in the pathogenesis of non-alcoholic steatohepatitis. Turk J Gastroenterol 2003, 14:228–233
52. Machado MV, Ravasco P, Jesus L, Marques-Vidal P, Oliveira CR, Proenca T, Baldeiras I, Camilo ME, Cortez-Pinto H: Blood oxidative stress markers in non-alcoholic steatohepatitis and how it correlates with diet. Scand J Gastroenterol 2008, 43:95–102
53. Wake K: "Sternzellen" in the liver: perisinusoidal cells with special reference to storage of vitamin A. Am J Anat 1971, 132:429–462
54. Purohit V, Abdelmalek MF, Barve S, Benevenga NJ, Halsted CH, Kaplowitz N, Kharbanda KK, Liu QY, Lu SC, McClain CJ, Swanson C, Zakhari S: Role of S-adenosylmethionine, folate, and betaine in the treatment of alcoholic liver disease: summary of a symposium. Am J Clin Nutr 2007, 86:14–24
55. Martínez-Chantar ML, Vazquez-Chantada M, Ariz U, Martinez N, Varela M, Luka Z, Capdevila A, Rodriguez J, Aransay AM, Matthiesen R, Yang H, Calvisi DF, Esteller M, Fraga M, Lu SC, Wagner C, Mato JM: Loss of the glycine N-methyltransferase gene leads to steatosis and hepatocellular carcinoma in mice. Hepatology 2008, 47:1191–1199
56. Wortham M, He L, Gyamfi M, Copple BL, Wan YJ: The transition from fatty liver to NASH associates with SAMe depletion in db/db mice fed a methionine choline-deficient diet. Dig Dis Sci 2008, 53:2761–2774
57. Lu SC, Alvarez L, Huang ZZ, Chen L, An W, Corrales FJ, Avila MA, Kanel G, Mato JM: Methionine adenosyltransferase 1A knockout mice are predisposed to liver injury and exhibit increased expression of genes involved in proliferation. Proc Natl Acad Sci USA 2001, 98:5560–5565
58. Mato JM, Lu SC: Role of S-adenosyl-L-methionine in liver health and injury. Hepatology 2007, 45:1306–1312
59. Park YM, Febbraio M, Silverstein RL: CD36 modulates migration of mouse and human macrophages in response to oxidized LDL and may contribute to macrophage trapping in the arterial intima. J Clin Invest 2009, 119:136–145
60. Bataller R, Schwabe RF, Choi YH, Yang L, Paik YH, Lindquist J, Qian T, Schoonhoven R, Hagedorn CH, Lemasters JJ, Brenner DA: NADPH oxidase signal transduces angiotensin II in hepatic stellate cells and is critical in hepatic fibrosis. J Clin Invest 2003, 112:1383–1394
61. Wheeler MD, Kono H, Yin M, Nakagami M, Uesugi T, Arteel GE, Gabele E, Rusyn I, Yamashina S, Froh M, Adachi Y, Iimuro Y, Bradford BU, Smutney OM, Connor HD, Mason RP, Goyert SM, Peters JM, Gonzalez FJ, Samulski RJ, Thurman RG: The role of Kupffer cell oxidant production in early ethanol-induced liver disease. Free Radic Biol Med 2001, 31:1544–1549
62. Rallidis LS, Drakoulis CK, Parasi AS: Pravastatin in patients with nonalcoholic steatohepatitis: results of a pilot study. Atherosclerosis 2004, 174:193–196
63. Hyogo H, Tazuma S, Arihiro K, Iwamoto K, Nabeshima Y, Inoue M, Ishitobi T, Nonaka M, Chayama K: Efficacy of atorvastatin for the treatment of nonalcoholic steatohepatitis with dyslipidemia. Metabolism 2008, 57:1711–1718